frontiers in Climate

TYPE Original Research
PUBLISHED 03 July 2026
DOI 10.3389/fclim.2026.1853116

OPEN ACCESS

EDITED BY
Ben W. Kolosz,
University of Hull, United Kingdom

REVIEWED BY
Mark Mba Wright,
Iowa State University, United States
Chenxia Su,
Chinese Academy of Sciences (CAS), China

*CORRESPONDENCE
Johannes Meyer zu Drewer
✉ mzd@ithaka-institut.org
Nikolas Hagemann
✉ hagemann@ithaka-institut.org;
✉ nikolas.hagemann@agroscope.admin.ch

RECEIVED 11 April 2026
REVISED 04 May 2026
ACCEPTED 06 May 2026
PUBLISHED 03 July 2026

CITATION
Meyer zu Drewer J, Vorrath M-E, Amann T, Hartmann J, Ansari M, Cárcamo Pérez M and Hagemann N (2026) Combining biochar and basanite rock powder enhances carbon dioxide removal by carbonate alkalinity production. *Front. Clim.* 8:1853116. doi: 10.3389/fclim.2026.1853116

Combining biochar and basanite rock powder enhances carbon dioxide removal by carbonate alkalinity production

Johannes Meyer zu Drewer[1,2,3]*, Maria-Elena Vorrath[4], Thorben Amann[4], Jens Hartmann[4], Maria Ansari[4], Marcela Cárcamo Pérez[1] and Nikolas Hagemann[1,2]*

[1]Ithaka Institute, Goldbach, Germany, [2]Environmental Analytics, Agroscope, Zürich, Switzerland, [3]Institute of Sustainable Energy Systems (INES), Offenburg University, Offenburg, Germany, [4]Department of Earth System Sciences, University of Hamburg, Hamburg, Germany

Introduction: The combination of enhanced rock weathering (ERW) with pyrogenic carbon capture and storage (PyCCS) has been proposed to harness synergistic effects on carbon dioxide removal (CDR). Synergies may arise from co-application of silicate rock powder and biochar, or from co-pyrolysis of rock powder and biomass to produce rock-enhanced (RE-)biochar. While co-pyrolysis with silicate rock powder is well documented not to affect the carbon yield nor the aromaticity of RE-biochar, the effect of co-pyrolysis and co-application on alkalinity production by ERW remains poorly constrained.

Methods: We quantified the daily and cumulative production of carbonate alkalinity (TA_{carb} g^{-1} basanite) in a controlled weathering experiment conducted in columns, comparing 14 treatments consisting of basanite rock powder, biochar, co-applications or RE-biochars produced at contrasting highest treatment temperatures (HTT) of 450 °C and 750 °C. The experiment was run under two conditions: sandy, agricultural topsoil under ambient pCO_2, and washed, quasi non-reactive quartz sand under elevated pCO_2, the latter designed to better isolate leachate signals originating from the amendments alone. Column flushing with demineralized water prior to the experiment and subtraction of TA_{carb} signals from the matrix material and biochar amendments enabled quantification of the net TA_{carb} signal from ERW, here referred to as Net_TA_{carb}. Complementary pseudo-lysimeter experiments (i.e., the same treatments set up in larger vegetated soil columns) were used to assess effects on plant growth.

Results: Cumulative Net_TA_{carb} production was significantly higher from co-deployments than from pure basanite ($p < 0.05$), with RE-biochars producing more alkalinity than co-applications under both pCO_2 regimes. Thermal treatment of pure basanite increased its mean specific surface area ($p > 0.05$) but decreased its Net_TA_{carb} production. The release of dissolved silica correlated with Net_TA_{carb} production. In the pseudo-lysimeter experiments, no significant effect of any amendment on plant growth was observed.

Discussion: Carbon sinks from PyCCS and ERW have complementary sequestration curves. Silicate rock powder may therefore be co-deployed with biochar to hedge carbon losses from biochar mineralization while increasing alkalinity production and unlocking additional agronomic co-benefits.

KEYWORDS

CDR, co-pyrolysis, enhanced rock weathering, ERW, mineral-enriched biochar, PyCCS, rock-enhanced biochar

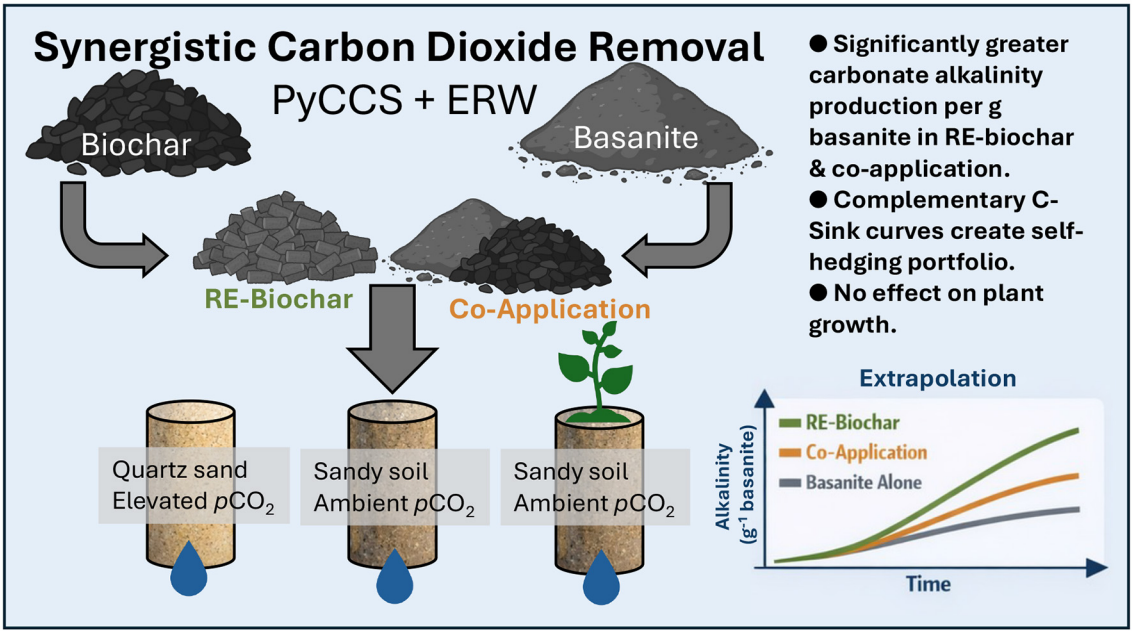

GRAPHICAL ABSTRACT

Highlights

- Thermal treatment of basanite did not increase its alkalinity production.
- Co-application and co-pyrolysis increase alkalinity production significantly.
- Separate quantification of alkalinity produced by biochar.
- Strong correlation of alkalinity and silica leaching.
- No significant effects of amendments on plant growth.

1 Introduction

The limitation of global warming to below 2 °C compared to pre-industrial levels requires significant reductions of anthropogenic CO_2 emissions (IPCC, 2023). However, global decarbonization has been delayed, such that ambitious climate targets can now only be met by combined pathways of emission reductions and carbon dioxide removal (CDR) from the atmosphere (Smith et al., 2024). One proposed CDR approach is enhanced rock weathering (ERW), which accelerates natural silicate weathering by applying finely ground silicate rock powder to land, typically agricultural soils (Hartmann et al., 2013; Moosdorf et al., 2014; Strefler et al., 2018; Haque et al., 2019; Beerling et al., 2020, 2025). Atmospheric CO_2 dissolves in water forming a weak carbonic acid ($CO_2(aq) + H_2O \rightarrow H_2CO_3$), which hydrolyzes the soil-applied silicate minerals — a process known as chemical weathering. Reaction products include bicarbonate (HCO_3^-) — a form of dissolved inorganic carbon (DIC), dissolved geogenic cations, dissolved silica (DSi), and in some instances secondary minerals. This mechanism is illustrated for orthoclase, a potassium (K) feldspar (Equation 1) and forsterite, a magnesium (Mg) bearing olivine (Equation 2) as follows (modified from Hartmann et al., 2013):

$$2KAlSi_3O_8(s) + 2CO_2(aq) + 11H_2O \rightarrow Al_2Si_2O_5(OH)_4(s) + 2K^+(aq) + 2HCO_3^-(aq) + 4H_4SiO_4(aq) \quad (1)$$

$$Mg_2SiO_4(s) + 4CO_2(aq) + 4H_2O \rightarrow 2Mg^{2+}(aq) + 4HCO_3^-(aq) + H_4SiO_4(aq) \quad (2)$$

Each mol of produced bicarbonate corresponds to one mol of dissolved CO_2 and thus one mol of atmospheric CO_2 removed. Depending on the solution's pH, some proportion of DIC is present as carbonate, which reduces the efficiency of the CO_2 transfer into alkalinity. The sum of bicarbonate and carbonate ion charges is referred to as carbonate alkalinity (TA_{carb}), making up most of the total alkalinity (TA, Renforth, 2019). The TA, along with the released cations, increases the acid buffer capacity (also referred to as alkalinity) of the soil solution. It is exported from soils via groundwater and rivers to the ocean, where it remains for millennia (Renforth and Henderson, 2017).

In recent years, ERW received extensive attention both regarding its benefits for agro-ecosystems (Haque et al., 2019; Almaraz et al., 2021; Swoboda et al., 2022; Cong et al., 2024) and its CDR potential (Beerling et al., 2020; Lewis et al., 2021; Larkin et al., 2022; te Pas et al., 2023). Multiple factors were identified that influence the rock weathering rate: (i) water availability (Kump et al., 2000; Strefler et al., 2018; Cipolla et al., 2021; Kanzaki et al., 2022; Deng et al., 2023); (ii) mineral speciation (Goldich, 1938; Deng et al., 2023;

Hermanská et al., 2022, 2023); (iii) particle size distribution and specific surface area (SSA) of the rock powder available for reactions (Israeli and Emmanuel, 2018; Rinder and von Hagke, 2021; Amann et al., 2022); (iv) CO_2 partial pressure (pCO_2) and soil solution pH (Gudbrandsson et al., 2011; Amann et al., 2022); (v) soil temperature (Gudbrandsson et al., 2011; Xu et al., 2024); and (vi) the activity of soil biota (Dontsova et al., 2020; Samuels et al., 2020; Vicca et al., 2022; Sohng et al., 2025).

Biochar is the solid, porous material obtained from biomass pyrolysis consisting of highly recalcitrant pyrogenic carbon (PyC). Its production from sustainably sourced biomass and subsequent non-oxidative use, e.g., as soil amendment, is a CDR approach referred to as pyrogenic carbon capture and storage (PyCCS; Schmidt et al., 2019, 2021). Soil-applied biochar can increase the soil water-holding capacity (Ali et al., 2017) and improve drainage (Vorrath et al., 2025), potentially facilitating weathering reactions and the export of TA_{carb}. Biochar can stimulate microbial activity and respiration, increasing soil pCO_2 (Palansooriya et al., 2019). The co-application of biochar with silicate rock powder therefore holds promise for synergistic CDR effects (Amann and Hartmann, 2019; Hagens et al., 2023). Rock-enhanced (RE-)biochar is the solid product of co-pyrolysis of biomass with (silicate) rock. This thermal treatment of the rock can (i) increase its specific surface area (SSA) due to fracturing (Mahanta et al., 2016; Jiang et al., 2022); (ii) change the speciation and thus solubility of minerals, like serpentines (Du Breuil et al., 2019; Kelemen et al., 2011, 2020; Buss et al., 2024), and (ii) passivate reactive rock surfaces by pyrogenic carbon coatings (Meyer zu Drewer et al., 2025). Both co-pyrolysis and co-application can lead to a strong (temporal) increase in soil pH (Meyer zu Drewer et al., 2025; Vorrath et al., 2025), which can reduce the weathering reactions of many minerals (White and Brantley, 1995) and is therefore typically undesired in the context of ERW.

The effects of co-application and co-pyrolysis on weathering rates, carbonate alkalinity production, and net CDR have not yet been quantified. Here, we investigated the production of TA_{carb} in controlled weathering experiments and compared 14 treatments comprising individual application of basanite rock powder and wood-derived biochar, their co-application and respective RE-biochars, produced at 450 °C and 750 °C. Additionally, the same treatments were set-up in a complementary pseudo-lysimeter experiment planted with alfalfa (*Medicago sativa* L.). The present study complements existing work on RE-biochar and biochar–basanite co-applications (Maslouski et al., 2025; Meyer zu Drewer et al., 2025; Vorrath et al., 2025) by systematically varying pyrolysis temperature and biomass-to-rock ratio, and by applying a controlled weathering protocol that includes pre-experimental column flushing and a Net_TAcarb correction framework. The goals of this study were to (i) test if thermal treatment of basanite increases alkalinity production, (ii) quantify the contribution of biochar to alkalinity production, (iii) quantify the potential effect of plants on ERW and (iv) assess how co-pyrolysis and co-application modify the temporal development of alkalinity production and the overall carbon sink (C-sink) created.

TABLE 1 Basic properties of the sandy soil used in the ambient pCO_2 controlled weathering experiment and the pseudo-lysimeter trial.

Property	Value
Sand fraction (%)	93.8
Silt fraction (%)	2.5
Clay fraction (%)	3.7
Total carbon (%)	1.2
Total inorganic carbon (%)	0.04
Organic carbon (%)	1.2
Total nitrogen (%)	0.1
pH—in deionized water, 1:2.5 mass ratio	5.6
pH—in 0.01 M $CaCl_2$, 1:2.5 mass ratio	4.7
EC—in deionized water, 1:2.5 mass ratio (µS cm^{-1})	47.7
Cation exchange capacity (mmol kg^{-1})	21.0
Base saturation (%)	140.7*
Water holding capacity (%)	30.0

*Base saturation >100% = Soil contains more basic cations (Mg, Ca, K, Na) than can be held by the soil colloids cation exchange capacity. For example, extractable cations from residual mineral fertilizer or soil organic matter.
EC = electrical conductivity (salinity) measured in solution.

TABLE 2 Basic properties of the pristine basanite rock powder.

Property	Value
Grain size range (µm)	0–250
p80 diameter (µm)	62.0
Specific surface area (m^2 g^{-1})	3.5
SiO_2 (% as oxide)	43.6
MgO (% as oxide)	8.9
CaO (% as oxide)	12.1
Na_2O (% as oxide)	2.9
K_2O (% as oxide)	3.5
P_2O_5 (% as oxide)	0.6
SO_3 (% as oxide)	0.1
∑AAEM-oxides (% as oxide)	27.4
Carbon sink potential (kg CO_2e t^{-1} rock)*	383

*Calculated according to equation S5, additional text S2, including ocean re-equilibration. Further characterization of mineralogy and thermally treated basanite in Supplementary Table 1. AAEM = alkali- and alkaline earth metals. p80 diameter = 80 mass-% of the sample is smaller than the p80 diameter.

2 Materials and methods

2.1 Soil, sand and rock

Sandy topsoil (0–20 cm, Table 1) was sourced from a field of Gräflich Bernstorff'sche Betriebe in Gartow, Germany (53°1′14″N 11°0′05″E), and analyzed as described in additional text S2. Quartz filter sand (0.4–0.8 mm, Mituso, Hamburg, Germany) was washed with deionized water (MilliQ) until the supernatant reached an EC < 5 µS cm^{-1}. Basanite rock powder "Eifelgold" (Table 2) was taken from the same batch as in previous studies (Supplementary Table 2

in Meyer zu Drewer et al., submitted[1]) and was used pristine or after thermal treatment on the PYREKA research pyrolysis unit (Pyreg GmbH, Dörth, Germany) with 15 min residence time and no added biomass (Meyer zu Drewer et al., submitted) (see text footnote 1). Pristine and thermally treated rock powders were analyzed by X-ray diffraction (XRD; D8 Advance, Bruker Corporation, Billerica, USA, performed by Qmineral, Leuven, Belgium) and Fourier-transform infrared spectroscopy (FTIR; Invenio X, Bruker Corporation) in attenuated total reflectance mode. The SSA was quantified in triplicate from N_2 adsorption isotherms (DIN ISO 9277:2014). Water-extractable alkali- and alkaline earth metals (AAEMs; Supplementary Table 1) were measured by ICP-OES according to DIN EN ISO 17294-2 after 1 h extraction of powder with ultrapure water (1 + 9 by mass) at 150 rpm. Extractions were conducted in triplicate, and eluates were analyzed by Eurofins Umwelt-Ost GmbH (Bobritzsch-Hilbersdorf, Germany).

2.2 Rock-enhanced biochar

We used (RE-)biochars produced and characterized by Meyer zu Drewer et al., submitted (see text footnote 1) (Supplementary Table 4 therein). In brief, woody biomass (*Picea abies* L.; Allspan German Horse GmbH, Karlsruhe, Germany; 0.4% ash; 50.6% organic carbon; C_{org}), was homogenized and pelletized with basanite rock powder from the same batch as used in the present study, and pyrolyzed using a PYREKA research pyrolysis unit (PYREG GmbH, Dörth, Germany, Hagemann et al., 2020) at 450 °C or 750 °C HTT. This procedure yielded (RE-)biochars with rock content of 0% (BC450, BC750), 50% (e.g., BC450-1:1), or 90% (e.g., BC750-1:9). All RE-biochars were analyzed by Eurofins Umwelt-Ost GmbH (Bobritzsch-Hilsdorf, Germany, Table 3) following the analytical guidelines of the European Biochar Certificate (EBC, 2025).

2.3 Controlled weathering experiment

Following the principal set-up of Amann et al. (2022) and (Vorrath et al., 2025), acrylic tubes (length: 25 cm, inner diameter 5.6 cm) were sealed at the bottom with a 5 µm mesh plankton net (Hydro-Bioas, Altenholz, Germany) and used as columns. Two series of $n = 20$ columns each were filled according to treatments described in Table 4: an ambient pCO_2 series with sandy soil (proxy for real world conditions) and an elevated pCO_2 series with washed quartz sand designed to minimize soil background leaching, signal delay and enhance rock weathering rate. The influence of soil properties on ERW was beyond the scope of this study.

The column set-ups were normalized by volume. We homogeneously incorporated 140 ml amendments (~30 vol-%) into 350 ml matrix material (~70 vol-%) resulting in a mean filling volume of 439±31 cm^3 per column. The total volume varied slightly (standard deviation < 10% of mean) because amendments occupied the pore space of the matrix material to varying degrees. The volume-normalized set-up was chosen over a mass-normalized set-up to achieve a more comparable total pore volume and water holding capacity (WHC, Supplementary Figure 1) despite the contrasting bulk densities of basanite rock powder (~2.6 g cm^{-3}) and biochar (~0.2 g cm^{-3}).

Columns in the ambient pCO_2 series were exposed to indoor air, for which CO_2 concentration was assumed to be around 0.045%. The elevated pCO_2 series was run inside a glovebox (further referred to as incubator), where CO_2 concentration was increased by flushing with pure CO_2 three times a week. However, leakage could not be avoided. The actual CO_2 concentration was calculated from the leachate pH, DIC and major cations of the unamended quartz sand control using PHREEQC (Parkhurst and Appelo, 2013; version 3.7.3.1596; database: phreeqc.dat). This indicated a mean CO_2 concentration of 42.4 ± 6.0% (Supplementary Figure 2). Both series were run without vegetation and in the dark. The mean temperature for both experiments was 17.5 ± 1.8 °C.

In week 0, prior to starting the experiment, each column was flushed with 1400 ml MilliQ water (<5 µS cm^{-1}; 280 ml day^{-1}; corresponding to seven times the WHC of the sandy topsoil) to remove the soluble fraction of biogenic ash and carbonates from the biochar (Meyer zu Drewer et al., 2025), as well as dissolved organic carbon (DOC) from both biochar and soil. Total alkalinity and major cations (Mg^{2+}, Ca^{2+}, K^+, Na^+) release during this period are reported in Supplementary Tables 2 and 3. Saturated column weights were used to calculate the relative (% of dry weight) and absolute (ml) WHC (Supplementary Figure 2). Following the flushing, columns were incubated for 189 days and irrigated manually with 25.5 ml MilliQ water three times per week (Monday, Wednesday, Friday). The target cumulative irrigation volume was 2045 ml per column, equivalent to 831 mm precipitation per half-year. In the ambient pCO_2 series, the columns "Control" and "R" (replicate 2) showed a clogging of pores in week six, resulting in lower water flow and leachate volumes. Overall irregularities (human errors) in the manual irrigation schedule were negligible, mean cumulative irrigation was 2,004 ± 71 ml in the ambient pCO_2 series and 2,053 ± 12 ml in the elevated pCO_2 series. Leachate was collected in flasks beneath the columns. The soil columns under ambient pCO_2 conditions were covered with aluminum foil caps to minimize evaporation. This was not necessary in the incubator as the vapor pressure deficit in a closed system is minimal.

2.4 Leachate analysis

Cumulative leachate was collected and analyzed in eight intervals (day 14, 28, 42, 63, 84, 105, 147, 189). For the elevated pCO_2 experiment, samples were collected and transferred to closed vials directly in the incubator to prevent CO_2 outgassing and precipitation of carbonates. Leachate pH, temperature and electric conductivity (EC) were measured immediately after sampling with a WTW 3630 IDS (Xylem Inc., San Diego, United States of America). Sub-samples for titration, ion chromatography and DSi quantification were filtered through 0.45 µm polyethersulfone (PES) syringe filters (Satorius Stedim Biotech, Göttingen, Germany), stored dark at 4 °C, and analyzed within 48 h.

1 Meyer zu Drewer, J., Bromm, T., Bucheli, T. D., Conte, P., de la Rosa, J. M., Fitzek, H., et al. (submitted). The hydrogen puzzle in rock-enhanced biochar: pyrogenic coating, mineral redox and pore accessibility. *PLoS One*.

TABLE 3 Basic physico-chemical properties of biochar and rock-enhanced biochar produced at 450 °C or 750 °C highest treatment temperature (BC450/BC750). Rock-enhanced biochars contain 50% (1:1) or 90% (1:9) basanite. Data from Meyer zu Drewer et al., submitted (see text footnote **1**).

Property	BC 450	BC 450-1:1	BC 450-1:9	BC 750	BC 750-1:1	BC 750-1:9
Mass conversion (y_m%)*	24.2	37.4	59.5	17.6	29.9	69.0
Carbon yield (y_c%)*	41.7	44.2	36.9	32.7	30.4	40.4
Rock content (%)*	0	50.2	89.1	0	49.9	89.1
Biogenic content (%)*	100	49.8	10.9	100	50.1	10.9
Total ash (%)	1.9	51.2	89.3	3.0	51.3	89.4
Biogenic ash (%)	1.9	1.0	0.2	3.0	1.4	0.3
C (%)	87.2	46.4	9.3	94.1	42.8	10.6
C_{org} (%)	87.2	46.4	9.3	93.9	42.8	10.6
C_{org_daf} (% of C_{org})	88.9	95.1	86.9	96.8	87.9	100.0**
BC_{HyPy} (% of C_{org})***	56.4	49.5	42.7	97.3	97.4	97.2
TIC (%)	< 0.1	< 0.1	< 0.1	0.2	< 0.1	< 0.1
H (%)	3.1	1.6	0.6	1.1	0.7	0.6
N (%)	0.44	0.30	0.18	0.65	0.36	0.22
S (%)	< 0.03	< 0.03	< 0.03	< 0.03	< 0.03	< 0.03
O (%)	7.4	0.5	0.6	1.1	4.9	−0.8**
H:C_{org} molar ratio	0.42	0.41	0.77	0.14	0.19	0.67
H_{Bio}:C_{org} molar ratio	0.42	0.37	0.43	0.14	0.15	0.37
CaO (%)	0.59	5.79	9.73	0.94	5.90	10.01
K_2O (%)	0.24	1.79	2.86	0.33	1.80	2.95
MgO (%)	0.10	4.30	7.95	0.18	4.57	7.69
Na_2O (%)	0.03	1.69	2.86	0.04	1.64	2.86
P_2O_5 (%)	0.06	0.31	0.54	0.09	0.31	0.54
MnO (%)	0.07	22.07	39.38	0.11	22.26	39.43
SiO_2 (%)	0.18	0.15	0.18	0.30	0.15	0.18
Cu (mg kg^{-1})	3	35	56	6	35	54
Ni (mg kg^{-1})	<1	61	94	7	71	93
Zn (mg kg^{-1})	35	60	73	10	54	71

*Calculated according to additional text S2.

**Calculated using the samples ash content. The treatment BC750-1:9 has a very high ash content and proportional error. A slight overestimation of the ash content (measurement error) can lead to $C_{org\_daf} \geq 100\%$ and oxygen $\leq 0\%$.

***Persistent carbon fraction (BC_{HyPy}) as determined by hydropyrolysis. The hydro pyrolysis data is adopted from Table 1 in Meyer zu Drewer et al., submitted (see text footnote 1) who used the same raw materials and pyrolysis conditions.

Daf, dry and ash free; TIC, total inorganic carbon; H_{Bio}, biogenic hydrogen.

Total alkalinity was measured by automated titration (Titrando, Metrohm, Filderstadt, Germany) to pH 4.3 with 0.02 M HCl following Dickson (1981). Major cations (Mg^{2+}, Ca^{2+}, K^+, Na^+, NH_4^+) and anions (SO_4^{2-}, Cl^-, F^-, NO_3^-, NO_2^-) were quantified by ion chromatography on a Metrohm 881 Compact IC Pro system (Metrohm, Filderstadt, Germany). The charge balance error (CBE%) was calculated from the quantified load of cations and anions (including TA) and their specific valence. Dissolved silica was quantified using a UV-VIS spectrophotometer (DR 6000, Hach Lange GmbH, Düsseldorf, Germany) by measuring absorbance at 810 nm. Samples were prepared by acidification (3.6 M H_2SO_4) and addition of a molybdate reagent to form silicomolybdous acid, which was subsequently reduced with ascorbic acid to produce a blue-colored indicator compound (Nieuwenhuize et al., 1994). Dissolved inorganic carbon was measured on a Picarro Carbon Isotope Analysis System (Picarro Inc., Santa Clara, California, USA) which performs automated acidification to convert DIC into CO_2 to be collected and quantified. Carbonate alkalinity (TA_{carb}) was calculated based on measured temperature, DIC, pH, and major cation concentrations using PHREEQC (Parkhurst and Appelo, 2013; database: phreeqc.dat). Organic alkalinity (TA_{org}) was defined as the difference between TA and TA_{carb}.

2.5 Calculation of net alkalinity production and data extrapolation

The TA_{carb} signal of ERW is driven by the release of geogenic cations. To isolate this signal, TA_{carb} contributions from the

TABLE 4 Matrix material (sandy topsoil or washed quartz sand), basanite powder, biochar, rock-enhanced biochar and corresponding load of pyrogenic carbon (PyC) from amendments in the volume-normalized columns (70 vol-% matrix material, 30 vol-% amendment) of the controlled weathering experiments. Note that minor mass-differences arise from heterogeneous particle size distributions within the standardized volume.

pCO_2	Treatment	Replicates	Matrix material (g)	Basanite powder (g)	Biochar (g)	RE-biochar (g)	PyC* (g)
Ambient	Control	1	674	0	0	0	0
Ambient	R	3	485	155	0	0	0
Ambient	R450	1	485	159	0	0	0
Ambient	R750	1	486	158	0	0	0
Ambient	BC450	1	486	0	67	0	59
Ambient	BC750	1	486	0	62	0	58
Ambient	BC450 + R_1:9	1	486	124	14	0	12
Ambient	BC450 + R_1:1	1	486	49	49	0	43
Ambient	BC750 + R_1:9	1	485	122	14	0	13
Ambient	BC750 + R_1:1	3	486	45	45	0	42
Ambient	RE-BC450_1:9	1	485	0	0	107	10
Ambient	RE-BC450_1:1	1	486	0	0	88	41
Ambient	RE-BC750_1:9	1	486	0	0	113	12
Ambient	RE-BC750_1:1	3	485	0	0	90	39
Elevated	Control	1	742	0	0	0	0
Elevated	R	3	524	158	0	0	0
Elevated	R450	1	533	160	0	0	0
Elevated	R750	1	532	153	0	0	0
Elevated	BC450	1	533	0	69	0	60
Elevated	BC750	1	532	0	62	0	59
Elevated	BC450 + R_1:9	1	532	125	14	0	12
Elevated	BC450 + R_1:1	1	533	49	49	0	43
Elevated	BC750 + R_1:9	1	533	122	14	0	13
Elevated	BC750 + R_1:1	3	533	47	48	0	45
Elevated	RE-BC450_1:9	1	533	0	0	109	10
Elevated	RE-BC450_1:1	1	532	0	0	91	42
Elevated	RE-BC750_1:9	1	533	0	0	112	12
Elevated	RE-BC750_1:1	3	532	0	0	85	36

*PyC, pyrogenic carbon, equal to organic carbon in biochar (cf. Table 3).
R, basanite rock powder; BC, biochar; 450/750, 450/750 °C highest treatment temperature during pyrolysis; RE-BC, rock-enhanced biochar; BC + R, co-applications; 1:9, 10% biochar to 90% basanite mass ratio; 1:1, 50% biochar to 50% basanite mass ratio.

soil matrix and biochar amendments—presumably originating from biogenic cation release (e.g., from soil organic matter or biochar ash)—were corrected for using Equations 3–5. First, TA_{carb} generated by the matrix material in the control columns was subtracted according to Equation 3:

$$TA_{carb\_a\_i} = (TA_{carb\_i} V_{l\_i}) - \frac{(TA_{carb\_ctrl} * V_{l\_ctrl})}{m_{m\_ctrl}} * m_{m\_i} \quad (3)$$

With $TA_{carb\_a\_i}$ being the amount of carbonate alkalinity produced by the amendment of treatment i in mmol, TA_{carb_i} the carbonate alkalinity produced by treatment i in mmol L^{-1}, V_{l_i} the leachate volume of treatment i in L, m_{m_i} the mass of the matrix material in treatment i in g. Subscript "*ctrl*" refers to measurements obtained from the unamended control (matrix material only) incubated under the respective pCO_2.

Based on TA_{carb_a} of the BC450 and BC750 treatments and the C_{org} content of these biochars, from here on referred to as pyrogenic carbon (PyC), we estimated alkalinity production per unit PyC according to Equation 4:

$$TA_{carb\_PyC} = \frac{TA_{carb\_a(BC)}}{m_{PyC}} \quad (4)$$

With TA_{carb_PyC} being the TA_{carb} produced by biochar amendments, expressed in µmol TA_{carb} g^{-1} PyC, $TA_{carb\_a(BC)}$ the TA_{carb} produced by BC450 or BC750 calculated according to Equation 3 and m_{PyC} the mass of PyC in the respective column in g.

For treatments combining rock and biochar, TA_{carb_a} was corrected for TA_{carb_PyC} and normalized to 1 g of basanite rock according to Equation 5:

$$Net\_TA_{carb\_i} = \frac{TA_{carb\_a\_i} - (TA_{carb_{PyC}} * m_{PyC_i})}{m_{rock\_i}} \quad (5)$$

With $Net\_TA_{carb\_i}$ (µmol g^{-1} rock) being the $TA_{carb\_a\_i}$ production of treatment *i*, corrected for alkalinity produced by the biochar amendments, TA_{carb_PyC} from Equation 4, m_{PyC_i} the mass PyC in treatment *i*, and m_{rock_i} the mass of basanite in treatment *i*, both given in g. The same mathematical operation as described in Equations 3–5 was also used to calculate the net release of DSi and AAEMs.

Cumulative Net_TA_{carb} (µmol g^{-1} rock) was converted to daily rates by division, considering the length of measurement interval, resulting in Net_TA_{carb} g^{-1} rock day^{-1}. The daily rate of Net_TA_{carb} production was extrapolated for 20 years to model the development of the inorganic carbon sink (IC-sink) generated from ERW, following the *"medium"* scenario suggested by Vorrath et al. (2025), which assumes a decrease of Net_TA_{carb} g^{-1} rock day^{-1} by 0.5% every 7^{th} day—starting from the end-point of empirical measurements. Extrapolations were performed for the triplicated treatments R, BC750+R_1:1 and RE-BC750_1:1 in sandy topsoil under ambient pCO_2 (proxy for real world conditions) and are reported per ton of basanite. One mol of Net_TA_{carb} produced was assumed to correspond to 0.85 mol CO_2e removed and stored, accounting for the re-equilibration of the ocean carbonate system (Equation S5 in additional text S2). The development of the biochar-based C-sink (PyC-sink) was modeled following the Global Biochar C-Sink (2026), where a two-pool exponential decay model is applied to the semi-persistent PyC fraction (semi-persistent fraction = 100% - persistent fraction; Equation S6-S7 in additional text S2). The persistent PyC fraction is here defined as the (RE-)biochars C_{org} content that is resistant to hydropyrolysis (BC_{HyPy}) and was set to 97% for BC750 and RE-BC750_1:1, according to the BC_{HyPy} content of comparable (RE-)biochars produced and analyzed by Meyer zu Drewer et al., submitted (see text footnote 1); Table 1 therein.

2.6 Pseudo-lysimeter trials with *Medicago sativa* L.

Seventy pseudo-lysimeters (height: 70 cm, inner diameter: 24 cm) were built from polyvinyl chloride (PVC) pipes. Each lysimeter was filled with 50 cm of soil layered on a fine sieve, through which leachate drained into a reservoir from where it was extracted by pump. First, 18.6 kg of soil (Table 1) were filled into the pseudo-lysimeter to form the lower 30 cm of the soil column. Second, 12.4 kg of the same soil were thoroughly mixed with 147 g (32.5 t ha^{-1}) of amendments in a concrete mixer for 60 s, which were then added to the column to form the upper 20 cm of the soil column. Treatments were set up in five replicates and arranged in a randomized complete block design. To keep the soil column constantly at 20 °C, pseudo-lysimeters were placed in water basins (Supplementary Figure 3) connected to a heat pump (IPSpro, Pool-Systems GmbH, Winklarn, Germany). The surrounding poly-tunnel was not heated.

Alfalfa (*Medicago sativa* L.; Kipenkerl, Bruno Nebelburg GmbH, Everswinkel, Germany) was sown at 30 seeds per lysimeter. One month after sowing, the pseudo-lysimeters received a basal fertilization by injection of diluted liquid fertilizer, equivalent to 40 kg N ha^{-1}, 64 kg P_2O_5 ha^{-1} and 96 kg K_2O ha^{-1}, also supplying essential micronutrients (Wuxal Top K, Hauert MANNA Düngerwerke GmbH, Nürnberg, Germany). We acknowledge that also mineral fertilizer can produce alkalinity, however this effect is constant across all treatments including the control and is thus negligible for treatment comparison. Two months after sowing additional 4.32 g H_3BO_3 were added to each lysimeter to correct a boron deficiency. Neem oil (1:111 dilution) and yellow sticky traps were used for pest control. Lysimeters were initially adjusted to 60% of WHC, then irrigated on demand. Once per month a heavy-rain event (equivalent to ≥33 L m^{-2}) was simulated (Supplementary Table 4).

The experiment lasted for 10 months (September 2023–June 2024). Leachate was sampled monthly (except March 2024) after the simulated heavy-rain events and analyzed for pH, EC, TA, and major ions as described above. Above-ground biomass (AGB) was harvested regularly by cutting the plants at 10 cm height. Below-ground biomass (BGB) was recovered by wet sieving at the end of the experiment. Biomass samples were dried for 24 h at 80 °C to determine the dry weight.

During the first 2 months of the experiment, irrigation was not yet fine-tuned and some lysimeters held no leachate at the day of sampling. To ensure balanced sample sizes these 2 months were removed from the dataset. Toward the end of the experiment, some lysimeters developed leaks that allowed water from the surrounding tank to enter the reservoir; the final 3 months were therefore also excluded from the leachate data set. The remaining data from November 2023 through February 2024 was further evaluated.

2.7 Statistics

We first fitted one-way ANOVA models and assessed ANOVA assumptions by testing residual normality (Q–Q plots, Shapiro–Wilk test) and variance homogeneity (Bartlett's and Brown–Forsythe tests). If these assumptions were met, ANOVAs were followed by Tukey HSD *post hoc* tests at $\alpha = 0.05$. For the pseudo-lysimeter trial, we applied repeated-measures ANOVA to account for the block design. All operations were facilitated by GraphPad Prism v10.4.1.

3 Results

3.1 Alkalinity and major ion release during the column flushing

Flushing proved to be a successful means to remove large shares of the biogenic cations from the columns prior to the experiment. Based on the triplicated treatments, the flushing period (week 0) accounted for 41–47% of total AAEM leaching in sandy soil columns and 10–29% in quartz sand columns (weeks 0–27). This corresponded to 29–38% and 6–18% of the entire TA produced (Supplementary Tables 2 and 3). The

TABLE 5 Initial pyrogenic carbon (PyC) content and cumulative alkalinity[a] production from biochar during the 27-week experiments.

C-sink property	Ambient pCO_2 experiment		Elevated pCO_2 experiment	
	BC450	BC750	BC450	BC750
PyC (%)[b]	87.2	93.9	87.2	93.9
TA_{PyC} (µmol g^{-1} PyC)	27.5	75.0	67.0	188.3
TA_{carb_PyC} (µmol g^{-1} PyC)	23.3	63.4	63.6	190.2
$TA_{biochar}$ (µmol g^{-1} biochar)	24.0	70.4	58.4	176.8
$TA_{carb\_biochar}$ (µmol g^{-1} biochar)	20.3	59.6	55.4	178.6
$TA_{PyC}/TA_{biochar}$	1.2	1.2	1.1	1.0
$TA_{carb\_PyC}/TA_{carb\_biochar}$	1.2	1.2	1.1	1.0

[a]The bulk alkalinity described here is exclusively of biogenic origin, i.e., produced by the biochar amendment. Still, it is not constrained by which mechanism the biochar contributed to the leachate alkalinity. These mechanisms may include the release of ionic forms of dissolved organic carbon, organic acids, biogenic cations, biogenic carbonates or the consumption of acidity due to the protonation of aromatic carbon moieties. Note that alkalinity per unit PyC and alkalinity per unit biochar are proportional, as the PyC to ash ratio of a given biochar is constant.
[b]PyC, organic biochar carbon (C_{org}).

comparison between basanite in quartz sand (treatment R, 6 µmol Net_AAEMs leaching g^{-1} amendment) and biochar in quartz sand (BC750, 89 µmol Net_AAEMs leaching g^{-1} amendment) highlighted that most AAEMs leached during flushing were biogenic. Notably, biochar controls in quartz sand suggest that ~20% and ~100% of total K was removed from BC450 and BC750, respectively, during flushing (BC450 = 69 g biochar with 0.20% K content and 648 µmol Net_K leached; BC750= 62 g biochar with 0.27% K content and 4503 µmol Net_K leached).

3.2 Carbonate alkalinity production

The cumulative TA_{carb} production (week 1–27) by the matrix material was 6.3 µmol g^{-1} sandy soil under ambient pCO_2 and 11.8 µmol g^{-1} quartz sand under elevated pCO_2. Cumulative TA and TA_{carb} production by the pure biochars are reported in Table 5. Data are expressed as alkalinity per gram PyC and per gram biochar; the two metrics are proportional since the PyC:ash ratio is fixed for each material. In general, TA exceeded TA_{carb}, TA_{carb} production was higher for BC750 than BC450, and elevated pCO_2 yielded greater TA_{carb} than ambient pCO_2.

Daily production of Net_TA_{carb} from R under ambient pCO_2 peaked within the first 14 days (0.3 ± 0 µmol TA_{carb} g^{-1} rock day^{-1}, Figure 1), while RE-BC750_1:1 and BC750+R_1:1 peaked by day 63 at 0.9 ± 0 and 0.7 ± 0 µmol TA_{carb} g^{-1} rock day^{-1}, respectively. Under elevated pCO_2, TA_{carb} production from R was rather constant throughout the experiment with mean 0.4 ± 0.4 µmol TA_{carb} g^{-1} rock day^{-1} over 189 days. Production of TA_{carb} by RE-BC750_1:1 and BC750+R_1:1 peaked at day 28 with 1.0 ± 0.5 and 0.7 ± 0.2 µmol TA_{carb} g^{-1} rock day^{-1}, respectively.

In HTT 750 °C treatments, TA_{carb} production from RE-biochar was mostly higher than those of co-application of biochar and rock powder. Differences were greater in the beginning (days 14–105), but rates converged toward the end of the experiment. In HTT 450 °C treatments, TA_{carb} production was similar for co-pyrolysis and co-application. Notably, after 189 days, TA_{carb} production from 1:1 co-applications and co-pyrolysis remained higher than that of pure rock treatment, with all treatments approaching a near steady state. Complementary chrono-sequences of AAEM leaching are provided in Supplementary Figures 4 and 5.

Despite an increase in mean SSA ($p = 0.06$) (Figure 2), there was a notable decrease in cumulative Net_TA_{carb} production when rock powder was thermally treated at 750 °C (Figures 3A, B). This is also mirrored in the fraction of water extractable AAEMs (∑Ca, Mg, K, Na) which decreased from 0.30% in R to 0.24% in both R450 and R750 (Supplementary Table 1). Thermal treatment at 450 °C had no effect on Net_TA_{carb} production of basanite rock powder.

Generally, cumulative Net_TA_{carb} production—normalized to rock powder mass—was greater in 1:1 treatments than in treatments containing 90% basanite. With few exceptions, the Net_TA_{carb} production from RE-biochars was higher than from mass-equivalent co-applications. Under ambient pCO_2, the Net_TA_{carb} production was greater from amendments produced at HTT 750 °C than from those at HTT 450 °C. Under elevated pCO_2, this trend was partly reversed.

Statistical evaluation of triplicated treatments revealed that Net_TA_{carb} production in µmol g^{-1} rock differs significantly between all compared treatments, with RE-BC750_1:1 (79.2 ± 3.1) > BC750 + R_1:1 (52.0 ± 10.3) > R (21.1 ± 4.1) under ambient pCO_2. The same sequence was observed under elevated pCO_2: RE-BC750_1:1 (128.2 ± 10.4) > BC750 + R_1:1 (95.4 ± 8.8) > R (70.6 ± 4.8; Figures 3A, B).

The combined effect of changing matrix material and increasing pCO_2 level promoted a stronger Net_TA_{carb} signal than detectable in sandy soil under ambient pCO_2. The treatments BC750+R_1:1 and BC750_1:1 in quartz sand under elevated pCO_2 produced the highest cumulative Net_TA_{carb}; 80% and 60% higher than their counterparts in the sandy soil + ambient pCO_2 series, respectively. While producing the least alkalinity overall, the Net_TA_{carb} production from pure basanite was increased tenfold in the elevated pCO_2 series, suggesting that pure basanite may be most sensitive to increases in pCO_2.

The amount of geogenic AAEMs leached (Figures 3C, D) largely mirrors the same pattern, with less pronounced differences between basanite in RE-biochars and co-applications. While

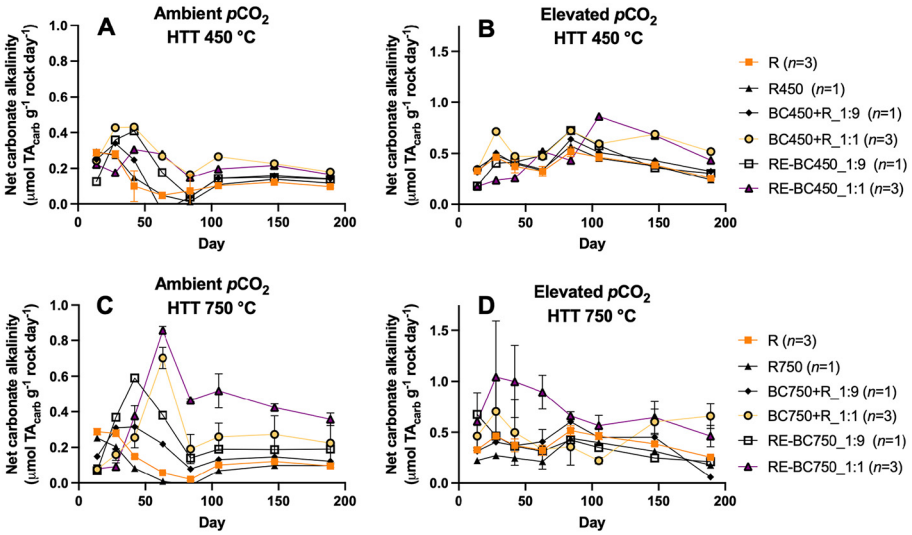

FIGURE 1
Daily rates of PHREEQC modeled carbonate alkalinity (TA_{carb}) production, corrected for TA_{carb} production by matrix material (quartz sand in panel **A** + **C**; sandy topsoil in panel **B** + **D**) and biochar amendments (Net_TA_{carb}), normalized to the mass of basanite rock. Treatments comprise basanite powder (R), biochar (BC) co-applied with rock (+R), and rock-enhanced biochar (RE-BC). The three-digit number indicates the temperature in °C during thermal treatment. The ratio refers to the mass ratio of biochar to rock. **(A)** Treatments produced at HTT 450 °C incubated under ambient pCO_2. **(B)** Treatments produced at HTT 450 °C under elevated pCO_2. **(C)** Treatments produced at HTT 750 °C under ambient pCO_2. **(D)** Treatments produced at HTT 750 °C under elevated pCO_2. The treatments R, BC750+R_1:1 and RE-BC750_1:1 (colored) are replicated with $n = 3$. Error bars indicate the standard deviation. For all other treatments $n = 1$ applies. Y-axis scales differ between ambient and elevated pCO_2 panels. A complementary chrono-sequence of geogenic alkali and alkaline earth metals (potassium, sodium, calcium, magnesium) leaching in µmol of charge g^{-1} rock day^{-1} (charge equivalents) is provided in Supplementary Figure 6.

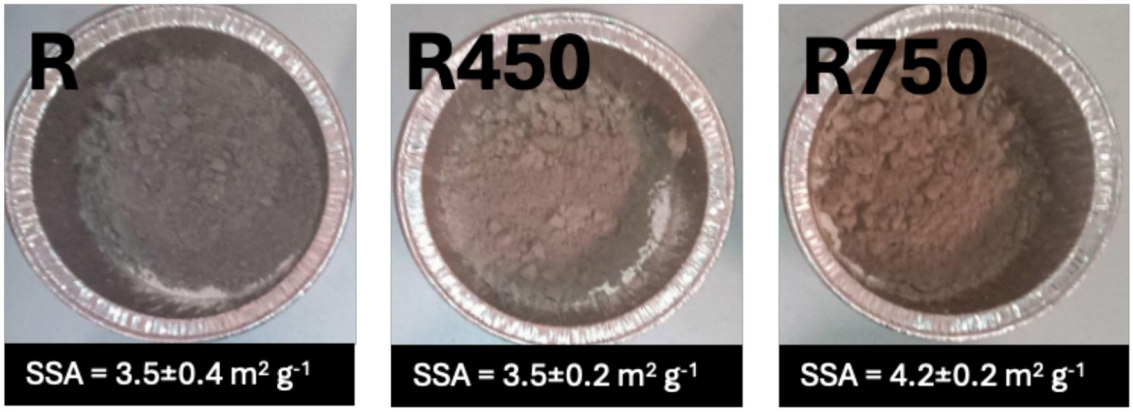

FIGURE 2
R: Pristine basanite rock powder, gray color. R450: Basanite rock powder thermally treated at 450 °C, reddish color. R750: Basanite rock powder thermally treated at 750 °C, reddish color. SSA = Specific surface area as determined from $n = 3$ replicates by N_2 adsorption following the Brunauer-Emmett-Teller method ($p = 0.06$); data adopted from Meyer zu Drewer et al., submitted (see text footnote 1).

the cumulative charge of geogenic AAEMs leached from RE-BC750_1:1 was significantly higher than from R ($p < 0.05$), co-pyrolysis vs. co-application under elevated pCO_2 and R vs. co-application under ambient pCO_2 were indifferent ($p > 0.05$). Assuming negligible rock weathering during the 5-day flushing period, cumulative AAEM losses amounted to 0–0.5% of the initial geogenic pool under ambient pCO_2 and 1–1.5% under elevated pCO_2 (Supplementary Figure 7). The treatment-specific mean CBE was ~10% in the ambient pCO_2 experiment (exceptions: Control = 24%; BC450 = 19%) and always < 4% in the elevated pCO_2 experiment, underscoring the overall good quality of the underlying data in the TA_{carb} modeling (Supplementary Figure 8). Though the CBE of the ambient pCO_2 control was higher than in other treatments, it did not fundamentally compromise TA_{carb} modeling. The same TA_{carb} trends were observed in the elevated pCO_2 experiment, consistently showing a lower CBE. The chrono-sequences of leachate pH, EC and DIC content are summarized in Supplementary Figures 9–11.

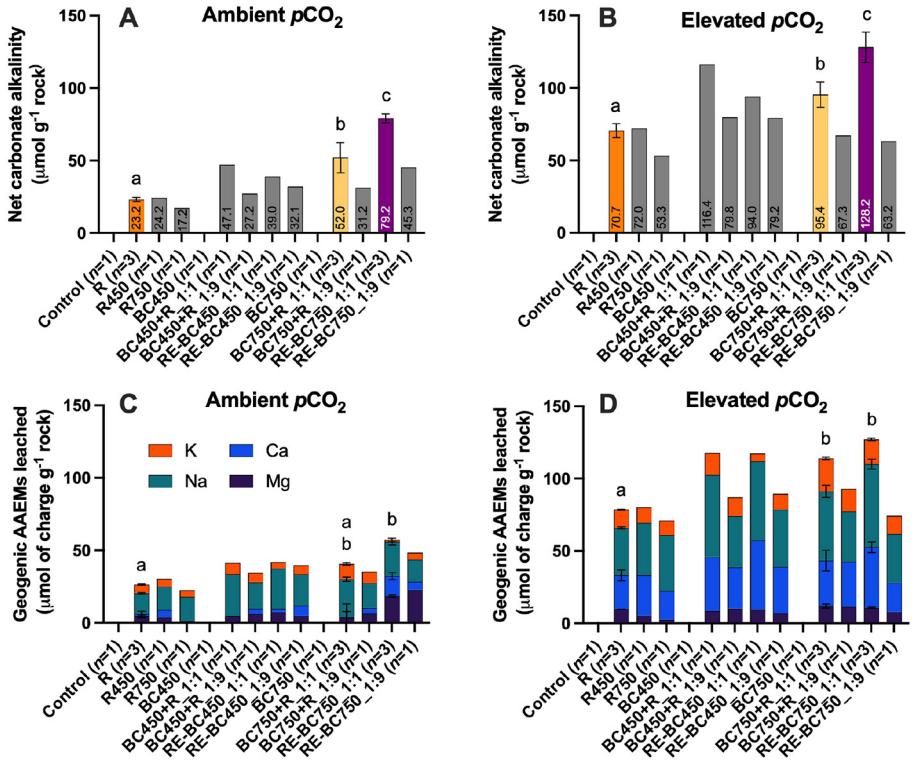

FIGURE 3
Production of net carbonate alkalinity (Net_TA_{carb}, µmol g^{-1} rock, **A, B**) and geogenic alkali and alkaline earth metals (AAEMs, µmol of charge g^{-1} rock, **C, D**) released during weathering of basanite powder (R), biochar (BC) co-applied with basanite (+R), and rock-enhanced biochar (RE-BC) during 189 days of column experiment. The three-digit number indicates the temperature in °C during thermal treatment. The ratio refers to the mass ratio of biochar to rock. The TA_{carb} was modeled using PHREEQC and leached AAEMs measured by ion-chromatography. Both TA_{carb} and AAEMs were corrected for signals produced by the matrix material and by the biochar amendments present in the respective columns, then normalized to the mass of basanite (Equations 3–5). (**A**+**C**)**:** Treatments under ambient pCO_2 in sandy topsoil. **(B, D):** Treatments under elevated pCO_2 (42.4±6.0%) in washed quartz sand. The treatments R, BC750+R_1:1 and RE-BC_750_1:1 are replicated with $n = 3$. Error bars indicate the standard deviation. For all other treatments $n = 1$ applies. For replicated treatments, homologous subgroups based on ANOVA with consecutive Tukey HSD post-hoc test (alpha = 0.05) are indicated in compact letter display.

3.3 Extrapolation of IC-sink and PyC-sink development

After 20 years, the modeled IC-sink for pure basanite, basanite in co-application and basanite in RE-biochar (sandy topsoil, ambient pCO_2) corresponded to 1.6%, 3.7% and 5.7% of the stoichiometric CDR maximum (CDR_{max}; 383 kg CO_2e t^{-1} rock; Table 6). One ton of BC750 had an initial PyC-sink of 3.44 t CO_2e, decreasing to 3.40 t CO_2e after 20 years. The same assumption for PyC decay was applied for BC750 in co-application and co-pyrolysis. The increasing IC-sink and decreasing PyC-sink complement each other, resulting in a near constant carbon sequestration over time (Figure 4).

3.4 Dissolved silica leaching

To evaluate DSi as a possible indicator of ERW, we related cumulative Net_DSi to Net_TA_{carb} per gram rock, both corrected for background signals from the matrix material. The DSi background signal was strong from the sandy topsoil (earlier cultivated with Si-rich *Poaceae* ssp.), whereas DSi release from woody biochar was negligible (Supplementary Figure 12). Across all treatments, cumulative Net_DSi and Net_TA_{carb} were significantly positively correlated under both pCO_2 regimes. Linear regressions fitted to these data (Figure 5) yielded a strong relationship under elevated pCO_2 ($R^2 = 0.84$) but a weaker one ($R^2 = 0.33$) under ambient pCO_2 when also outliers (green in Figure 5) were included in the analysis. The three outliers belong to the treatment RE-BC750-1:1 where Net_TA_{carb} and Net_DSi appear decupled, their exclusion resulted in R^2 of 0.55.

3.5 Plant performance and alkalinity production in the pseudo-lysimeter experiment

Mean total AGB was 429 ± 36 g dry weight per lysimeter (Supplementary Figure 13) and did not differ significantly between treatments. Mean BGB was 39 ± 13 g dry weight with no treatment effect, but significant block effect.

The quantification of alkalinity production from the pseudo-lysimeters remained challenging. As the pumping of the leachate

TABLE 6 C-sink potential and development of the inorganic C-sink (IC-sink from enhanced rock weathering) and pyrogenic carbon C-sink (PyC-sink from biochar) and total C-sink (sum of IC-sink and PyC-sink) after 20 years.

C-sink property	1 t basanite	1 t basanite in BC750 + R_1:1	1 t basanite in RE-BC750_1:1
CDR_{max} (kg CO_2e t^{-1} rock)[a]	383	383	383
IC-sink after 20 years (kg CO_2e t^{-1} rock)[b]	6 ± 0 (1.6% CDR_{max})	14 ± 5 (3.7% CDR_{max})	22 ± 2 (5.7% CDR_{max})
Initial PyC-sink (kg CO_2e t^{-1} biochar)[c]	0	3,443	3,443
PyC-sink after 20 years (kg CO_2e t^{-1} biochar)[d]	0	3,409	3,409
Total C-sink after 20 years (kg CO_2e)[e]	6 ± 0	3,423 ± 5	3,430 ± 2
Longterm total C-sink (kg CO_2e)[f]	192	3,532	3,532
Biomass C requirement (t biomass C t^{-1} PyC)[g]	n.a.	3,058	3,289

[a]Calculated based on equation S5 in additional text S2.
[b]Modeled according to section 2.5. The values are presented as mean ± standard deviation based on three replicates used for model parameterization.
[c]Based on 1 t BC750 at 94% C_{org} with 97% BC_{HyPy} (persistent carbon fraction; values adopted from Meyer zu Drewer et al., submitted (see text footnote 1).
[d]Modeled according to the Global Biochar C-Sink (2026).
[e]Sum of IC-sink and PyC-sink in year 20.
[f]Defined as PyC-sink of BC_{HyPy} + 50% CDR_{max} (Conservative buffer of 50% to the long-term IC-sink development).
[g]Calculated based on pyrolysis carbon yield (y_c) and organic carbon content (C_{org}) of the RE-biochar.
CDR_{max}, Maximum stoichiometric C-sink potential of a given rock in t CO_2e t^{-1} rock. n.a., not applicable.

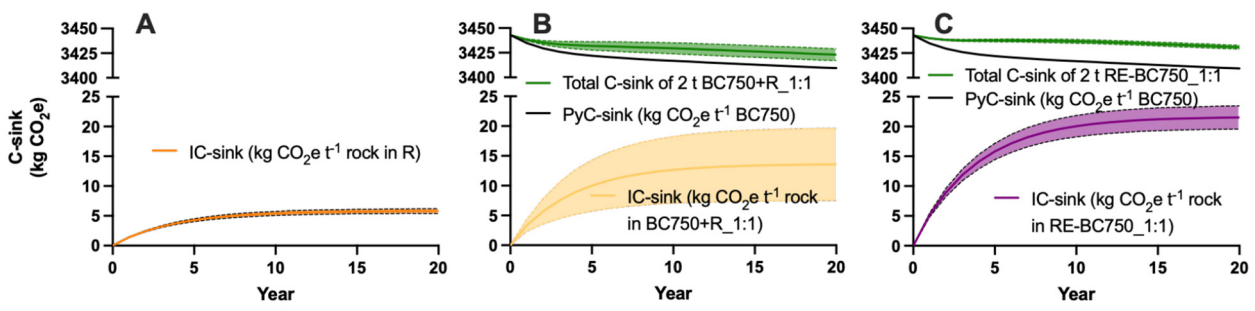

FIGURE 4
A 20-year extrapolation of the development of the inorganic carbon sink (IC-sink) in t CO_2e t^{-1} rock from enhanced rock weathering. Models were parameterized using the end-point of daily Net_TA_{carb} production (day 189) of the triplicated treatments R (1 t basanite, **(A)**), BC750+R_1:1 (1 t basanite in co-application with 1 t of 750 °C biochar, **(B)**) and RE-BC750_1:1 (1 t basanite co-pyrolyzed with biomass resulting in 1 t of 750 °C biochar, **(C)**). Only data from treatments using sandy soil under ambient pCO_2 were selected to serve as a proxy for real world conditions. The mean IC-sink is plotted as a line with standard deviation based on $n = 3$ replicates as shaded area. The PyC-sink development (1 t BC750) is indicated in black. The total C-sink development of 2 t BC750+R_1:1 and RE-BC750_1:1 (IC-sink based on 1 t basanite in RE-biochar of co-application + PyC-sink based on 1 t 750 °C biochar) are indicated in green.

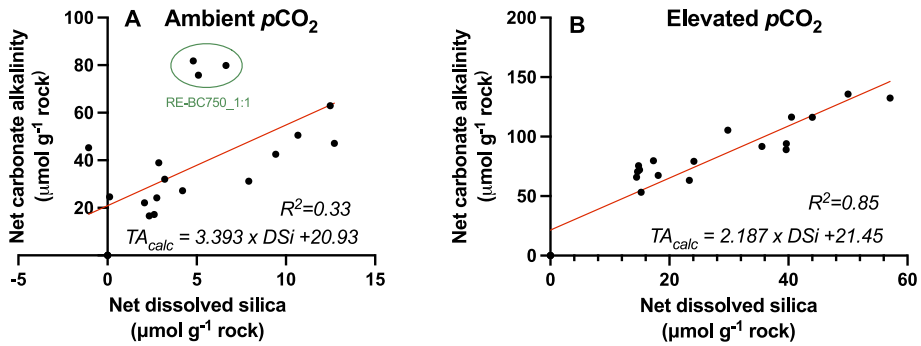

FIGURE 5
Correlation of cumulative carbonate alkalinity (Net_TA_{carb}) and dissolved silica (Net_DSi), both presented in µmol g^{-1} rock and corrected for background signals from the matrix material. Correlation based on $n = 20$ columns monitored under ambient **(A)** and elevated pCO_2 **(B)**. A linear regression is indicated in red with R^2 as comparative measure of fit and regression function. Note the differently scaled Y-axis between ambient and elevated pCO_2.

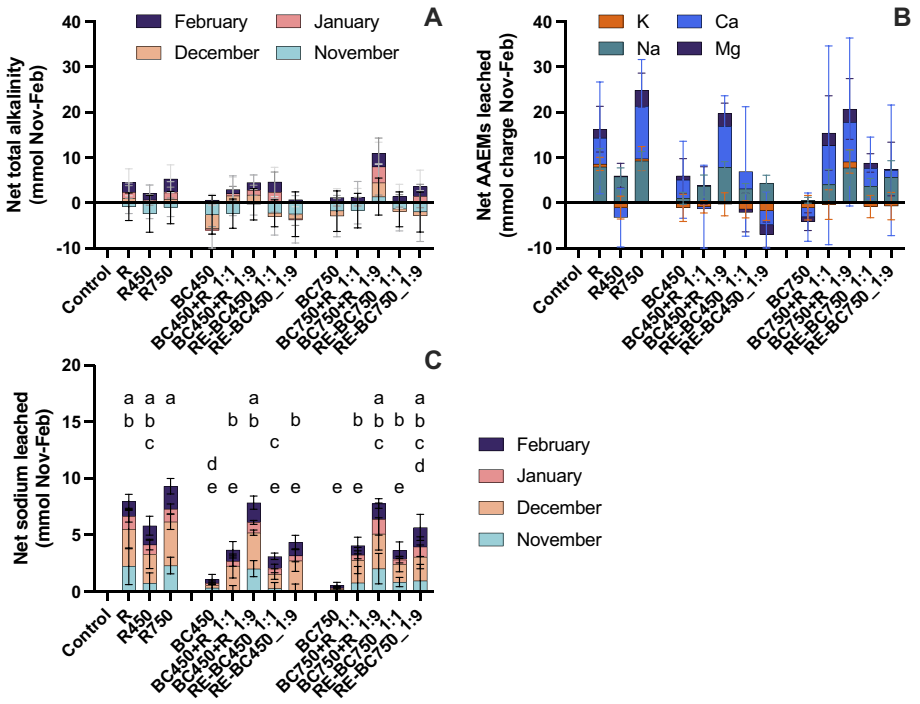

FIGURE 6
Data obtained from leachate analysis in the pseudo-lysimeter experiment. **(A)** Cumulative total alkalinity production presented in mmol. **(B)** Cumulative leaching of alkali and alkaline earth metals (AAEM) presented in mmol of charge. **(C)** Cumulative leaching of sodium (Na) in mmol. Treatments comprise basanite powder (R), biochar (BC) co-applied with basanite (+R), and rock-enhanced biochar (RE-BC). The three-digit number indicates the temperature in °C during thermal treatment. The ratio refers to the mass ratio of biochar to rock. Data is corrected for the matrix signal and covers the time between November 2023 and February 2024. Data is presented as mean based on $n = 5$ replicates ± standard deviation. Homologous subgroups based on repeated-measures ANOVA with consecutive Tukey HSD *post-hoc* test (alpha = 0.05) are indicated in compact letter display.

water can lead to degassing of CO_2, it was not possible to measure DIC and to model TA_{carb}. The matrix signal dominated both the titrated TA and leached AAEMs (Figure 6), yielding a mean of 15 mmol TA and releasing AAEMs equivalent to 34 mmol charge. These mean figures are based on the cumulative signal over four sampling events (November-February). Correcting for this strong matrix signal resulted in net negative values for alkalinity production, cumulative AAEM leaching, or both, depending on the treatment. With 25 mmol of charge, R750 resulted in the highest mean Net_AAEM leaching, followed by co-applications with 90% basanite. However, there was no significant difference in Net_TA $\Sigma_{Nov-Feb}$ or Net_AAEMs charge equivalents $\Sigma_{Nov-Feb}$ between treatments. Only the ion-specific comparison of Na leaching indicated a significant treatment effect. Sodium leaching was significantly higher from R, R450 and R750, same as combined treatments containing 90% basanite (Figure 6C). Gross leaching data on Na, K, Ca and Mg as well as chrono-sequences of leachate pH and EC are provided in Supplementary Figures 14 and 15, respectively.

4 Discussion

4.1 Partitioning of matrix- and rock-powder-derived alkalinity

Flushing the columns revealed a significant proportion of non-ERW-derived alkalinity in the columns with RE-biochar or biochar/rock-powder co-applications. Alkalinity can be generated by background weathering of soil minerals but also by biogenic cations and dissolved organic materials producing "*organic*" alkalinity (TA_{org}). However, where bicarbonate is charge-balanced by compounds such as conjugated organic acids or biogenic cations the CDR can neither be considered permanent nor additional (Kerr et al., 2021, 2023; Lee et al., 2024; Vorrath et al., 2025; Rieder et al., 2026). Accurate separation of the alkalinity signal derived from basanite weathering depends on comprehensive knowledge of background alkalinity (Maslouski et al., 2025).

During the flushing, the alkalinity from woody RE-biochars was dominated by K release, which is in line with previous short-term leaching experiments using RE-biochar (Meyer zu Drewer et al.,

2025; Vorrath et al., 2025). Flushing removed up to 100% of K from the high temperature biochar (750 °C), which is consistent with previous observations that K availability in biochars is increasing with HTT (Xiu et al., 2023). In the controlled weathering experiment—following the flushing—the release of AAEMs was now dominated by Na (Figure 3). Although both biochar and basanite have a similar content of Na (Table 3 and Supplementary Table 1), the cumulative Na leaching correlates positively ($p < 0.0001$) with the mass of rock amendment but negatively ($p < 0.0001$) with the mass of biochar amendments in the columns (Supplementary Figure 16). Sodium is likely released from Na-rich minerals prone to fast weathering, such as leucite, nepheline, or plagioclase, all contained in basanite (Dupla et al., 2025). This strongly suggests that biochar was no longer the main driver of alkalinity production after the flushing, which is supported by the lower DIC, TA and TA_{carb} production from pure biochar treatments in the controlled weathering experiment compared to treatments containing rock powder (Supplementary Figure 17). Also, DOC released by organic amendments, which can contribute ~5% to the measured TA in form of TA_{org} (Rieder et al., 2026), was likely removed during flushing; however, DOC was not quantified here. In summary, the flushing process was essential to quantify the net ERW signal over the short incubation period of just 189 days.

4.2 Mechanisms affecting carbonate alkalinity production

Both co-application and co-pyrolysis increased the alkalinity production per gram of rock. The increase was stronger in 1:1 than in 1:9 mass ratio. With non-ERW alkalinity sources removed (flushing and mathematical subtraction of remaining matrix and biochar signal), this points to additional, biochar-mediated physicochemical drivers of rock weathering. These drivers seem more effective where the biochar content in the soil is high (1:1 vs. 1:9).

Literature suggests that biochar co-application can: (i) Enhance the soil WHC (Wei et al., 2023)—including rock powder amended domains (Supplementary Figure 1); (ii) Improve the matrix porosity and connectivity (Vorrath et al., 2025)—allowing better TA_{carb} export; (iii) Reversibly sorb cations (Munera-Echeverri et al., 2018)—lowering the soil solution's saturation index; and (iv) Increase the soil microbial activity and respiration (Palansooriya et al., 2019; te Pas et al., 2026)—producing additional CO_2 and lowering the soil pH.

Further, co-pyrolysis may be able to: (i) Increase the rock's SSA due to micro-fractures and the dehydration of minerals (Moura and Prado, 2009; Jiang et al., 2022); (ii) Change the speciation of minerals (Kelemen et al., 2011, 2020); (iii) Reduce metal-oxides during co-pyrolysis (Meyer zu Drewer et al., submitted) (see text footnote 1) and after soil application where biochar can act as electron shuttle and donator (Xu et al., 2019; Yuan et al., 2022); and (iv) Cause the pyrogenic coating of mineral surfaces with conducive secondary char (Meyer zu Drewer et al., 2025).

Other studies have predicted a tenfold increase in the weathering rate for some minerals after thermal treatment, e.g. due to the conversion of minerals from the serpentine group to minerals of the olivine group (Gerdemann et al., 2007; Dlugogorski and Balucan, 2014; Du Breuil et al., 2019). Meyer zu Drewer et al., submitted (see text footnote 1) proposed the mobilization of K from nepheline or leucite, as K was found in elevated concentrations at the biochar-mineral interface. Further, they described the reduction of trivalent iron oxide (hematite) during co-pyrolysis. While iron is not a contributor to alkalinity (dissolved iron species rapidly precipitate in soil under oxic conditions at circumneutral pH), pyrolytic redox-reactions can cause disruptions of the overarching mineral structure. Pyrogenic coatings as described by Meyer zu Drewer et al. (2025) apparently do not reduce weathering rates—contrary to the assumption that such coatings passivate reactive surfaces. Instead, we suggest that the layer of conductive secondary char may improve the shuttling of electrons in domains close to the rock particle surface and thus may facilitate redox reactions. The CEC of biochar can (reversibly) sorb cations, which would lower the mineral-specific saturation index of the soil solution and support mineral dissolution while preventing oversaturation and, e.g., calcite precipitation. In this study, neither mineral precipitation was observed nor a specific saturation index calculated. Nevertheless, the very high application rates of basanite in the controlled weathering experiment, ranging from ~185 t ha^{-1} (1:1 co-deployment) to 635 t ha^{-1} (basanite only), suggest that saturation effects could occur and slow down the reaction kinetics of ERW. Biochar can mitigate this effect by reversibly sorbing cations, improving matrix porosity and solute transport. Oversaturation is likely less of a constraint where realistic application rates of 10–50 t basanite ha^{-1} are employed.

While co-applications benefit ERW only through hydrological and microbial effects, ERW in RE-biochars can additionally benefit from altered mineral structure and composition—albeit likely restricted to superficial domains. The acceleration of ERW through altered mineral structure is thus transient as weathering consumes the modified components. At the same time, soil-structural and biological changes may persist, as reflected in the gradual convergence of Net_TA_{carb} production rates of co-applications and RE-biochar. Still, after 6 months, in both experiments, Net_TA_{carb} production rates were higher for 1:1 RE-biochars and co-applications compared to R. However, this was considerably less pronounced under elevated pCO_2. The elevated pCO_2 experiment likely provides a *"fast-forward"* picture of the long-term trajectory of the ambient experiment. As both matrix material and pCO_2 differed between series, comparisons are restricted to relative changes between treatments; a quartz-sand control under ambient pCO_2 would have allowed a more rigorous separation but was not part of the present design. Based on our limited data, we cannot conclude with certainty that beneficial effects of co-applications persist for extended time horizons (10–20 years).

4.3 Effect of thermal treatment on pure basanite

Pure basanite was thermally treated at 450 °C (R450) and 750 °C (R750) in a PYREKA pyrolysis unit without the addition of biomass. Basanite treated at 450 °C appears unaffected across all measured parameters. Thermal treatment at 750 °C reduced Net_TA_{carb} in the controlled weathering experiment despite an increase in mean SSA, although neither XRD

(Supplementary Table 1) nor FTIR (Supplementary Figure 18) could detect any pronounced changes in mineral composition. The observed decrease in TA_{carb} production may be attributed to other forms of thermal passivation, such as changes in surface chemistry leading to greater hydrophobicity. The latter could be investigated with X-ray photoelectron spectroscopy, which was beyond the scope of our study.

In contrast, in the pseudo-lysimeter experiment, R750 led to the highest AAEM leaching. While acknowledging the generally greater uncertainties in this experiment, the results suggest that possible passivation may be overcome in biologically active systems and that ERW benefits from the increased SSA. The increase in SSA may be an effect of the thermal reduction of trivalent iron (6% Fe_2O_3 in basanite, Clausen and Fabricius, 2000). Iron reduction in basanite was already observed following its thermal treatment, and more pronounced following co-pyrolysis (Meyer zu Drewer et al., submitted) (see text footnote 1). Additionally, the dehydration and detachment of phyllosilicates (3% 2:1-layer silicates in basanite, Heller-Kallai, 2006; Moura and Prado, 2009) or micro-fractures from thermal expansion may contribute to a greater mean SSA.

4.4 Sodium and DSi: proxies for weathering in complex systems?

Quantifying ERW-derived CDR via total or carbonate alkalinity in soils is difficult because weathering signals are delayed by cation exchange (te Pas et al., 2024; Dupla et al., 2025) and confounded by organic alkalinity (Rieder et al., 2026). At the same time TA_{carb} modeling requires substantial analytical efforts (Temperature, pH, IC, DIC).

We found that DSi correlates well with TA_{carb} and that significant differences in Na leaching can be detected where TA_{carb} or ΣAAEM signals remained undistinguishable. Generally, leachate DSi and Na are easy to measure. Dissolved silica and Na signals from woody biochar are unlikely to confound ERW signal (Supplementary Figures 4, 5, and 12). Further, due to its anionic form, DSi leaches easily at relevant soil pH (Schaller et al., 2021). Similarly, Na sorption to soil colloids is weak (Ca > Mg > K > Na) due to its low charge and large hydration radius. Therefore, these compounds are less prone to CEC-induced signal delay.

Still, rock weathering cannot simply be deduced stoichiometrically from DSi or Na leaching (e.g., by using normalized Si_1 or Na_1 stoichiometric formulae) as minerals are not subject to congruent dissolution and both Si and Na can be retained in secondary minerals (Amann et al., 2022). Further, both DSi and Na are subject to plant uptake (Hammes et al., 2025) and geogenic cations can displace native Na from soil colloids. Dissolved silica and Na may serve as proxies for qualitative comparisons within the same system. However, on their own, neither qualifies as a quantitative indicator ERW-derived CDR.

4.5 Interactions with plants in the pseudo-lysimeters

None of the amendments had a significant effect on plant growth in the pseudo-lysimeters. This observation aligns well with existing literature. Biochar tends to be less effective in promoting plant growth in temperate than in tropical agricultural systems (Jeffery et al., 2017). Also, the effect of ERW is highly site specific (Schiedung et al., 2026) and comparable pseudo-lysimeter studies, applying 50 t basalt ha^{-1} to temperate soils and crops, could not demonstrate an increased biomass accumulation (Vienne et al., 2022). A meta-analysis suggests that high application rates (>50 t ha^{-1}) may even have negative effects on soil chemistry—interpreted in the context of CDR and agriculture (Xu et al., 2025). The moderate rate applied here (32.5 t ha^{-1}) did not compromise the yield due to undesirable shifts in soil chemistry (e.g., pH or salinity spike).

The basanite contained only low concentrations of potentially toxic elements, in contrast to rocks used in other studies (Haque et al., 2020; Suhrhoff, 2022; Dupla et al., 2023). The soil originated from an organic farm with regular application of agricultural digestate; there was no evident micronutrient limitation that geogenic nutrients could have alleviated. Likewise, the frequent irrigation regime reduced the relevance of any biochar-induced changes in WHC (Ali et al., 2017; Wei et al., 2023). Potential stimulation of biological nitrogen fixation in legumes by biochar (Farhangi-Abriz et al., 2024) did not translate into detectable biomass responses or enhanced root-nodulation.

The pseudo-lysimeter experiment was intended to complement the controlled weathering experiment to compare ERW in the presence and absence of plants, but this approach proved difficult in practice. In the vegetated system, seasonally varying amounts of irrigation water had to be applied. At the same time evapotranspiration and consequently the amount of percolating water varied continuously—prohibiting any direct comparison. Unambiguous measurements of net alkalinity production were hard to obtain in this complex system containing large amounts of agricultural soil along with soil organic matter, active microbes and plants—all contributing to TA_{org}. The chosen correction model (subtraction of the control signal) often led to net negative results. At amendment rates equivalent to 0.4 mass-% in the pseudo-lysimeter, the matrix signal was often stronger and its noise exceeded the amendment signal, which could be better isolated in the controlled weathering experiment where amendments (30 vol-%) made up 10–25 mass-%.

In contrast, Net_AAEM leaching could be isolated more effectively than Net_TA (cf. Bijma et al., 2026). This reflects the weaker AAEM background signal and the low CEC of the soil (Table 1), allowing Net_AAEM release to serve as a rough proxy for ERW. Among the treatments combining biochar and basanite, co-applications containing 90% rock powder promoted the greatest mean release of additional geogenic AAEMs. Though not significant, this trend contrasts with the controlled weathering experiment, where RE-biochars containing 50% rock produced most TA_{carb}. Hydrological improvements (as expected in 1:1 mass ratio) may not have been relevant in this well-irrigated and well-drained pseudo-lysimeter experiment. Notably, the treatment BC750 led to net negative AAEM leaching, likely due to the high CEC of the biochar resulting in AAEM sorption and leaching retardation—an effect that may also partly explain the attenuated AAEM signals in other biochar-containing treatments.

To more clearly isolate TA signals and to foster a better understanding of phyto-accelerated ERW, follow up studies should

use an inert growing medium and consider the actual water demand of the vegetated system to benchmark the irrigation of complementary non-vegetated systems. Further the use of *in-situ* pore water sampler may be considered to obtained undisturbed samples for DIC measurements.

4.6 Complementary carbon sequestration curves

Generally, ERW and PyCCS have complementary carbon sequestration curves. The semi-persistent fraction of PyC is mineralized and lost as CO_2 over time (Azzi et al., 2024; Hagemann et al., 2025; Schmidt et al., 2025), whereas the IC-sink from ERW builds up over time (cf. Figure 4). A combination of ERW and biochar—accounted for in a portfolio of time-aligned and stacked sequestration curves—can hedge losses due to PyC-sink decay, providing constant negative climate forcing. Note that the modeled IC-sink is based on the TA_{carb} production during the last sampling interval of the controlled weathering experiment (thus has a rather high sensitivity) and that the ERW CDR efficiency factor of 0.85 carries its own uncertainty.

Under the conditions investigated, one ton of basanite may counterbalance the long-term decay of the non-BC_{HyPy} fraction of one ton high-temperature ($\geq$ 750 °C) biochar; however, this extrapolation is limited by the small underlying dataset and is unlikely to be universally applicable across different materials and sites. Pyrolysis conditions and resulting fraction of semi-persistent PyC remain most relevant. For example, BC450-based PyC-sinks would require more basanite as the (potential) decay of a 44% non-BC_{HyPy} fraction needs to be compensated (Table 3). Generally, the time-aligned stacking of carbon sequestration curves can serve as a tool to bundle various types of C-sinks with distinct temporal dynamics (permanent, temporary, increasing, decreasing, fluctuating) into stable CDR portfolios.

5 Conclusions

In the controlled weathering experiment, co-pyrolysis was shown to enhance rock weathering rates. However, all potential drivers discussed above, most likely affected only the rock surface. Thus, the acceleration may be transient and wear off in the short- to mid-term. Both co-applications and use of RE-biochar can alter soil properties such as hydrology or microbial activity in ways that may support ERW in the long-term. While the transient acceleration of rock weathering is unlikely to (economically) justify and offset the production effort of RE-biochar, co-applications of biochar and basanite can be recommended unreservedly.

The monitoring of carbonate alkalinity production in complex biotic systems remains challenging. A direct comparison of alkalinity production between the vegetated and non-vegetated system within the chosen experimental setup proved impossible. Future research on weathering should consider inert growing media and standardize both amendment rates and irrigation schemes. Further, an appropriate variation of the flushing protocol—as tested in the controlled weathering experiment—should be included to ease the separation of biogenic and geogenic cations.

While no significant agronomic effects were observed in the present study using soil from temperate climate, synergistic benefits from the co-deployment of biochar and silicate rock powder can be expected when applied to degraded (e.g., tropical) soils. This assumes that the target soil is either initially acidic—and thus likely to benefit from the alkalinity produced—or sufficiently pH-buffered to avoid adverse effects.

In a 1:1 mass ratio combination of high temperature biochar (750 °C) and basanite rock powder, the PyC-sink of the biochar is the main contributor to CDR. After 20 years of rock weathering, the IC-sink contributes < 1% to the total C-sink. Still, the slowly increasing IC-sink can compensate for losses from the PyC-sink. In this regard, PyCCS and ERW represent a promising combination of CDR approaches with complementary sequestration curves.

Data availability statement

The original contributions presented in the study are included in the article/Supplementary material, further inquiries can be directed to the corresponding authors.

Author contributions

JMzD: Conceptualization, Formal analysis, Investigation, Methodology, Visualization, Writing – original draft. M-EV: Investigation, Writing – review & editing. TA: Investigation, Writing – review & editing. JH: Funding acquisition, Methodology, Resources, Writing – review & editing. MA: Investigation, Writing – review & editing. MC: Investigation, Writing – review & editing. NH: Conceptualization, Funding acquisition, Methodology, Supervision, Writing – review & editing.

Funding

The author(s) declared that financial support was received for this work and/or its publication. This research project was funded by the Deutsche Forschungsgemeinschaft (DFG, German Research Foundation) – grant 467391808 to Nikolas Hagemann.

Acknowledgments

We greatly appreciate the support by the laboratory coordinators, technicians and student assistants at the department of Earth System Sciences at the University of Hamburg, Germany. Their support was vital to the maintenance of the controlled weathering experiment. Great thanks go to Peggy Bartsch, Tom Jäppinen, Ciera Aldrich, Irmak Gök, Lennard Stoeck and Ina Nipper. The Ithaka Institute would like to thank the Carbon Drawdown Initiative, and especially Dirk Pässler, for their support,

which enabled us to improve our greenhouse infrastructure for the pseudolysimeter experiment.

Conflict of interest

NH is a co-author of several Carbon Standards AG guidelines for the certification of biochar (EBC) and biochar-based carbon sinks (EBC C-Sink/Global Biochar C-Sink, Global Artisan C-Sink). JMzD and NH co-authored the Global Rock C-Sink Standard owned by Carbon Standards AG.

The remaining authors declare that the research was conducted in the absence of any commercial or financial relationships that could be construed as a potential conflict of interest.

The author JH declared that they were an editorial board member of Frontiers, at the time of submission. This had no impact on the peer review process and the final decision.

Generative AI statement

The author(s) declared that Generative AI was not used in the creation of this manuscript.

Any alternative text (alt text) provided alongside figures in this article has been generated by Frontiers with the support of artificial intelligence and reasonable efforts have been made to ensure accuracy, including review by the authors wherever possible. If you identify any issues, please contact us.

Publisher's note

All claims expressed in this article are solely those of the authors and do not necessarily represent those of their affiliated organizations, or those of the publisher, the editors and the reviewers. Any product that may be evaluated in this article, or claim that may be made by its manufacturer, is not guaranteed or endorsed by the publisher.

Supplementary material

The Supplementary Material for this article can be found online at: https://www.frontiersin.org/articles/10.3389/fclim.2026.1853116/full#supplementary-material

References

Ali, S., Rizwan, M., Qayyum, M. F., Ok, Y. S., Ibrahim, M., Riaz, M., et al. (2017). Biochar soil amendment on alleviation of drought and salt stress in plants: a critical review. *Environ. Sci. Pollut. Res.* 14, 12700–12712. doi: 10.1007/s11356-017-8904-x

Almaraz, M., Wong, M. Y., Geoghegan, E. K., and Houlton, B. Z. (2021). A review of carbon farming impacts on nitrogen cycling, retention, and loss. *Ann. N. Y. Acad. Sci.* 1505, 102–117. doi: 10.1111/nyas.14690

Amann, T., and Hartmann, J. (2019). Ideas and perspectives: synergies from co-deployment of negative emission technologies. *Biogeosciences* 16, 2949–2960. doi: 10.5194/bg-16-2949-2019

Amann, T., Hartmann, J., Hellmann, R., Pedrosa, E. T., and Malik, A. (2022). Enhanced weathering potentials-the role of *in situ* CO_2 and grain size distribution. *Front. Clim.* 4:929268. doi: 10.3389/fclim.2022.929268

Azzi, E. S., Li, H., Cederlund, H., Karltun, E., and Sundberg, C. (2024). Modelling biochar long-term carbon storage in soil with harmonized analysis of decomposition data. *Geoderma* 441:116761. doi: 10.1016/j.geoderma.2023.116761

Beerling, D. J., Kantzas, E. P., Lomas, M. R., Wade, P., Eufrasio, R. M., Renforth, P., et al. (2020). Potential for large-scale CO_2 removal via enhanced rock weathering with croplands. *Nature* 583, 242–248. doi: 10.1038/s41586-020-2448-9

Beerling, D. J., Reinhard, C. T., James, R. H., Khan, A., Pidgeon, N., Planavsky, N. J., et al. (2025). Challenges and opportunities in scaling enhanced weathering for carbon dioxide removal. *Nat. Rev. Earth Environ.* 6, 672–686. doi: 10.1038/s43017-025-00713-7

Bijma, J., Hagens, M., Hammes, J. S., Planavsky, N., Pogge von Strandmann, P. A. E., Reershemius, T., et al. (2026). Reviews and syntheses: carbon vs. cation based MRV of enhanced rock weathering and the issue of soil organic carbon. *Biogeosciences* 23, 53–75. doi: 10.5194/bg-23-53-2026

Buss, W., Hasemer, H., Sokol, N. W., Rohling, E. J., and Borevitz, J. (2024). Applying minerals to soil to draw down atmospheric carbon dioxide through synergistic organic and inorganic pathways. *Commun. Earth Environ.* 5, 1–11. doi: 10.1038/s43247-024-01771-3

Cipolla, G., Calabrese, S., Noto, L. V., and Porporato, A. (2021). The role of hydrology on enhanced weathering for carbon sequestration II. From hydroclimatic scenarios to carbon-sequestration efficiencies. *Adv. Water Resour.* 154:103949. doi: 10.1016/j.advwatres.2021.103949

Clausen, L., and Fabricius, I. (2000). BET measurements: outgassing of minerals. *J. Colloid Interface Sci.* 227, 7–15. doi: 10.1006/jcis.2000.6880

Cong, L., Lu, S., Jiang, P., Zheng, T., Yu, Z., Xiaoshu, L., et al. (2024). CO_2 sequestration and soil improvement in enhanced rock weathering: a review from an experimental perspective. *Greenhouse Gases Sci. Technol.* 14, 1122–1138. doi: 10.1002/ghg.2313

Deng, H., Sonnenthal, E., Arora, B., Breunig, H., Brodie, E., Kleber, M., et al. (2023). The environmental controls on efficiency of enhanced rock weathering in soils. *Sci. Rep.* 13, 1–10. doi: 10.1038/s41598-023-36113-4

Dickson, A. G. (1981). An exact definition of total alkalinity and a procedure for the estimation of alkalinity and total inorganic carbon from titration data. *Deep Sea Res. Part A. Oceanogr. Res. Papers* 28, 609–623. doi: 10.1016/0198-0149(81)90121-7

Dlugogorski, B. Z., and Balucan, R. D. (2014). Dehydroxylation of serpentine minerals: implications for mineral carbonation. *Renew. Sustainable Energy Rev.* 31, 353–367. doi: 10.1016/j.rser.2013.11.002

Dontsova, K., Chorover, J., and Balogh-Brunstad, Z. (2020). Plants as drivers of rock weathering. *Biogeochemical Cycles: Ecological Drivers and Environmental Impact* (Washington, DC: AGU Publications), 33–58. doi: 10.1002/9781119413332.ch2

Du Breuil, C., Pasquier, L. C., Dipple, G., Blais, J. F., Iliuta, M. C., Mercier, G., et al. (2019). Mineralogical transformations of heated serpentine and their impact on dissolution during aqueous-phase mineral carbonation reaction in flue gas conditions. *Minerals* 9:680. doi: 10.3390/min9110680

Dupla, X., Bertagni, M. B., and Grand, S. (2025). Three years of field trials indicate a sustained enhanced rock weathering signal with limited CO_2 removal. *Environ. Sci. Technol.* 59, 25751–25764. doi: 10.1021/acs.est.5c09820

Dupla, X., Möller, B., Baveye, P. C., and Grand, S. (2023). Potential accumulation of toxic trace elements in soils during enhanced rock weathering. *Eur. J. Soil Sci.* 74:e13343. doi: 10.1111/ejss.13343

EBC (2025). *European Biochar Certificate - Guidelines for a Sustainable Production of Biochar (version 10.5)*. Arbaz, Switzerland: Ithaka Institute.

Farhangi-Abriz, S., Ghassemi-Golezani, K., Torabian, S., and Qin, R. (2024). A meta-analysis to estimate the potential of biochar in improving nitrogen fixation and plant biomass of legumes. *Biomass Convers. Biorefin.* 14, 3293–3303. doi: 10.1007/s13399-022-02530-0

Gerdemann, S. J., O'Connor, W. K., Dahlin, D. C., Penner, L. R., and Rush, H. (2007). *Ex situ* aqueous mineral carbonation. *Environ. Sci. Technol.* 41, 2587–2593. doi: 10.1021/es0619253

Global Biochar C-Sink (2026). *Global Biochar C-Sink, Version 4*. Arbaz, Switzerland: Ithaka Institute.

Goldich, S. S. (1938). A study in rock-weathering. *J. Geol.* 46, 17–58. doi: 10.1086/624619

Gudbrandsson, S., Wolff-Boenisch, D., Gislason, S. R., and Oelkers, E. H. (2011). An experimental study of crystalline basalt dissolution from 2pH11 and temperatures from 5 to 75 °C. *Geochimica et Cosmochimica Acta* 75, 5496–5509. doi: 10.1016/j.gca.2011.06.035

Hagemann, N., Schmidt, H. P., Bucheli, T. D., Grafmüller, J., Vosswinkel, S., Herdegen, V., et al. (2025). Proxies for use in biochar decay models: hydropyrolysis, electric conductivity, and H/Corg molar ratio. *PLoS One* 20:e0330206. doi: 10.1371/journal.pone.0330206

Hagemann, N., Schmidt, H. P., Kägi, R., Böhler, M., Sigmund, G., Maccagnan, A., et al. (2020). Wood-based activated biochar to eliminate organic micropollutants from biologically treated wastewater. *Sci. Total Environ.* 730:138417. doi: 10.1016/j.scitotenv.2020.138417

Hagens, M., Hartmann, J., Vicca, S., and Beerling, D. J. (2023). Editorial: enhanced weathering and synergistic combinations with other CDR methods. *Front. Clim.* 5:1244396. doi: 10.3389/fclim.2023.1244396

Hammes, J. S., Hartmann, J., Barth, J. A. C., Linke, T., Smet, I., Hagens, M., et al. (2025). Pre-print: soil processes govern alkalinity and cation retention in enhanced weathering for carbon dioxide removal. *EGUsphere* 1–40. doi: 10.5194/egusphere-2025-5402

Haque, F., Chiang, Y. W., and Santos, R. M. (2020). Risk assessment of Ni, Cr, and Si release from alkaline minerals during enhanced weathering. *Open Agric.* 5, 166–175. doi: 10.1515/opag-2020-0016

Haque, F., Santos, R. M., Dutta, A., Thimmanagari, M., and Chiang, Y. W. (2019). Co-benefits of wollastonite weathering in agriculture: CO_2 sequestration and promoted plant growth. *ACS Omega* 4, 1425–1433. doi: 10.1021/acsomega.8b02477

Hartmann, J., West, A. J., Renforth, P., Köhler, P., de La Rocha, C. L., Wolf-Gladrow, D. A., et al. (2013). Enhanced chemical weathering as a geoengineering strategy to reduce atmospheric carbon dioxide, supply nutrients, and mitigate ocean acidification. *Rev. Geophys.* 51, 113–149. doi: 10.1002/rog.20004

Heller-Kallai, L. (2006). Chapter 7.2 thermally modified clay minerals. *Dev. Clay Sci.* 1, 289–308. doi: 10.1016/S1572-4352(05)01009-3

Hermanská, M., Voigt, M. J., Marieni, C., Declercq, J., and Oelkers, E. H. (2022). A comprehensive and internally consistent mineral dissolution rate database: part I: primary silicate minerals and glasses. *Chem. Geol.* 597:120807. doi: 10.1016/j.chemgeo.2022.120807

Hermanská, M., Voigt, M. J., Marieni, C., Declercq, J., and Oelkers, E. H. (2023). A comprehensive and consistent mineral dissolution rate database: part II: secondary silicate minerals. *Chem. Geol.* 636:121632. doi: 10.1016/j.chemgeo.2023.121632

IPCC (2023). "Climate change 2023: synthesis report," in *Contribution of Working Groups I, II and III to the Sixth Assessment Report of the Intergovernmental Panel on Climate Change* (Geneva, Switzerland: IPCC), 184.

Israeli, Y., and Emmanuel, S. (2018). Impact of grain size and rock composition on simulated rock weathering. *Earth Surf. Dyn.* 6, 319–327. doi: 10.5194/esurf-6-319-2018

Jeffery, S., Abalos, D., Prodana, M., Bastos, A. C., Van Groenigen, J. W., Hungate, B. A., et al. (2017). Biochar boosts tropical but not temperate crop yields. *Environ. Res. Lett.* 12:053001. doi: 10.1088/1748-9326/aa67bd

Jiang, Y., Zhou, L., Zhu, Z., Ma, L., Chen, J., Li, Y., et al. (2022). Research on dynamic cracking properties of cracked rock mass under the effect of thermal treatment. *Theor. Appl. Fract. Mech.* 122:103580. doi: 10.1016/j.tafmec.2022.103580

Kanzaki, Y., Zhang, S., Planavsky, N. J., and Reinhard, C. T. (2022). Soil cycles of elements simulator for predicting TERrestrial regulation of greenhouse gases: SCEPTER v0.9. *Geosci. Model Dev.* 15, 4959–4990. doi: 10.5194/gmd-15-4959-2022

Kelemen, P. B., Matter, J., Streit, E. E., Rudge, J. F., Curry, W. B., Blusztajn, J., et al. (2011). Rates and mechanisms of mineral carbonation in peridotite: natural processes and recipes for enhanced, *in situ* CO_2 capture and storage. *Annu. Rev. Earth Planet. Sci.* 39, 545–576. doi: 10.1146/annurev-earth-092010-152509

Kelemen, P. B., McQueen, N., Wilcox, J., Renforth, P., Dipple, G., Vankeuren, A. P., et al. (2020). Engineered carbon mineralization in ultramafic rocks for CO2 removal from air: review and new insights. *Chem. Geol.* 550:119628. doi: 10.1016/j.chemgeo.2020.119628

Kerr, D. E., Brown, P. J., Grey, A., and Kelleher, B. P. (2021). The influence of organic alkalinity on the carbonate system in coastal waters. *Marine Chem.* 237:104050. doi: 10.1016/j.marchem.2021.104050

Kerr, D. E., Turner, C., Grey, A., Keogh, J., Brown, P. J., Kelleher, B. P., et al. (2023). OrgAlkCalc: estimation of organic alkalinity quantities and acid-base properties with proof of concept in Dublin Bay. *Marine Chem.* 251:104234. doi: 10.1016/j.marchem.2023.104234

Kump, L. R., Brantley, S. L., and Arthur, M. A. (2000). Chemical weathering, atmospheric CO_2, and climate. *Annu. Rev. Earth Planet. Sci.* 28, 611–667. doi: 10.1146/annurev.earth.28.1.611

Larkin, C. S., Andrews, M. G., Pearce, C. R., Yeong, K. L., Beerling, D. J., Bellamy, J., et al. (2022). Quantification of CO_2 removal in a large-scale enhanced weathering field trial on an oil palm plantation in Sabah, Malaysia. *Front. Clim.* 4:959229. doi: 10.3389/fclim.2022.959229

Lee, C. H., Lee, K., Lee, J. S., Jeong, K. Y., and Ko, Y. H. (2024). Persistent organic alkalinity in the ocean. *Geochimica et Cosmochimica Acta* 387, 53–62. doi: 10.1016/j.gca.2024.06.010

Lewis, A. L., Sarkar, B., Wade, P., Kemp, S. J., Hodson, M. E., Taylor, L. L., et al. (2021). Effects of mineralogy, chemistry and physical properties of basalts on carbon capture potential and plant-nutrient element release via enhanced weathering. *Appl. Geochem.* 132:105023. doi: 10.1016/j.apgeochem.2021.105023

Mahanta, B., Singh, T. N., and Ranjith, P. G. (2016). Influence of thermal treatment on mode I fracture toughness of certain Indian rocks. *Eng. Geol.* 210, 103–114. doi: 10.1016/j.enggeo.2016.06.008

Maslouski, M., Ansari, M., Hamburger, S. E., Meyer zu Drewer, J., Hagemann, N., Eschenbach, A., et al. (2025). Long-term carbon dioxide removal potential from the application of wood biochar and basanite rock powder in sandy soil using the LiDELSv2 process-based modeling approach. *Environ. Res. Lett.* 20:124032. doi: 10.1088/1748-9326/ae21f6

Meyer zu Drewer, J., Vorrath, M. E., Amann, T., Hartmann, J., De la Rosa, J. M., Möllmer, J., et al. (2025). Pyrogenic carbon and carbonating minerals for carbon capture and storage (PyMiCCS) part I: production, physico-chemical characterization and C-sink potential. *Front. Clim.* 7:1631368. doi: 10.3389/fclim.2025.1631368

Moosdorf, N., Renforth, P., and Hartmann, J. (2014). Carbon dioxide efficiency of terrestrial enhanced weathering. *Environ. Sci. Technol.* 48, 4809–4816. doi: 10.1021/es4052022

Moura, A. O., and Prado, A. G. S. (2009). Effect of thermal dehydration and rehydration on Na-magadiite structure. *J. Colloid Interface Sci.* 330, 392–398. doi: 10.1016/j.jcis.2008.10.032

Munera-Echeverri, J. L., Martinsen, V., Strand, L. T., Zivanovic, V., Cornelissen, G., Mulder, J., et al. (2018). Cation exchange capacity of biochar: an urgent method modification. *Sci. Total Environ.* 642, 190–197. doi: 10.1016/j.scitotenv.2018.06.017

Nieuwenhuize, J., Maas, Y. E. M., and Middelburg, J. J. (1994). Rapid analysis of organic carbon and nitrogen in particulate materials. *Marine Chem.* 45, 217–224. doi: 10.1016/0304-4203(94)90005-1

Palansooriya, K. N., Wong, J. T. F., Hashimoto, Y., Huang, L., Rinklebe, J., Chang, S. X., et al. (2019). Response of microbial communities to biochar-amended soils: a critical review. *Biochar* 1, 3–22. doi: 10.1007/s42773-019-00009-2

Parkhurst, D. L., and Appelo, C. A. J. (2013). "Description of input and examples for PHREEQC version 3: a computer program for speciation, batch-reaction, one-dimensional transport, and inverse geochemical calculations," in *U.S. Geological Survey Techniques and Methods* (Denver: U.S. Geological Survey), 497. doi: 10.3133/tm6A43

Renforth, P. (2019). The negative emission potential of alkaline materials. *Nat. Commun.* 10:1401. doi: 10.1038/s41467-019-09475-5

Renforth, P., and Henderson, G. (2017). Assessing ocean alkalinity for carbon sequestration. *Rev. Geophys.* 55, 636–674. doi: 10.1002/2016RG000533

Rieder, L., Hagens, M., Poetra, R., Vidal, A., Calogiuri, T., Neubeck, A., et al. (2026). Contribution of dissolved organic carbon to total alkalinity in enhanced weathering experiments. *Appl. Geochem.* 198:106685. doi: 10.1016/j.apgeochem.2026.106685

Rinder, T., and von Hagke, C. (2021). The influence of particle size on the potential of enhanced basalt weathering for carbon dioxide removal—insights from a regional assessment. *J. Cleaner Prod.* 315:128178. doi: 10.1016/j.jclepro.2021.128178

Samuels, T., Bryce, C., Landenmark, H., Marie-Loudon, C., Nicholson, N., Stevens, A. H., et al. (2020). "Microbial weathering of minerals and rocks in natural environments," in *Biogeochemical Cycles: Ecological Drivers and Environmental Impact* (Washington, DC: American Geophysical Union), 59–79. doi: 10.1002/9781119413332.ch3

Schaller, J., Puppe, D., Kaczorek, D., Ellerbrock, R., and Sommer, M. (2021). Silicon cycling in soils revisited. *Plants* 10:295. doi: 10.3390/plants10020295

Schiedung, M., Harrington, K. J., Dupla, X., Möller, B., Facq, E., Sweere, T., et al. (2026). Uncertainties of enhanced rock weathering for climate-change mitigation. *Nat. Rev. Earth Environ.* 7, 253–266. doi: 10.1038/s43017-026-00761-7

Schmidt, H. P., Abiven, S., Cowie, A., Glaser, B., Joseph, S., Kammann, C., et al. (2025). Biochar permanence-a policy commentary. *GCB Bioenergy* 17:e70092. doi: 10.1111/gcbb.70092

Schmidt, H. P., Anca-Couce, A., Hagemann, N., Werner, C., Gerten, D., Lucht, W., et al. (2019). Pyrogenic carbon capture and storage. *GCB Bioenergy* 11, 573–591. doi: 10.1111/gcbb.12553

Schmidt, H. P., Kammann, C., Hagemann, N., Leifeld, J., Bucheli, T. D., Sánchez Monedero, M. A., et al. (2021). Biochar in agriculture—a systematic review of 26 global meta-analyses. *GCB Bioenergy* 13, 1708–1730. doi: 10.1111/gcbb.12889

Smith, S. M., Geden, O., Gidden, M. J., Lamb, W. F., Nemet, G. F., Minx, J. C., et al. (eds.) (2024). *The State of Carbon Dioxide Removal 2024*, 2nd edn. Oxford: University of Oxford. doi: 10.17605/OSF.IO/F85QJ

Sohng, J., Sokol, N. W., Whiteaker, S., Schmidt, R., Holzer, I., Goertzen, H., et al. (2025). Combining organic amendments with enhanced rock weathering shifts soil carbon storage in croplands. *Sci. Total Environ.* 998:180179. doi: 10.1016/j.scitotenv.2025.180179

Strefler, J., Amann, T., Bauer, N., Kriegler, E., and Hartmann, J. (2018). Potential and costs of carbon dioxide removal by enhanced weathering of rocks. *Environ. Res. Lett.* 13:034010. doi: 10.1088/1748-9326/aaa9c4

Suhrhoff, T. J. (2022). Phytoprevention of heavy metal contamination from terrestrial enhanced weathering: can plants save the day? *Front. Clim.* 3:820204. doi: 10.3389/fclim.2021.820204

Swoboda, P., Döring, T. F., and Hamer, M. (2022). Remineralizing soils? The agricultural usage of silicate rock powders: a review. *Sci. Total Environ.* 807:150976. doi: 10.1016/j.scitotenv.2021.150976

te Pas, E. E. E. M., Chang, E., Marklein, A. R., Comans, R. N. J., and Hagens, M. (2024). Accounting for retarded weathering products in comparing methods for quantifying carbon dioxide removal in a short-term enhanced weathering study. *Front. Clim.* 6:1524998. doi: 10.3389/fclim.2024.1524998

te Pas, E. E. E. M., Comans, R. N. J., Bisseling, S., and Hagens, M. (2026). Enhanced weathering and biochar co-deployment boosts CO2 sequestration through changing soil properties. *Geoderma* 466:117668. doi: 10.1016/j.geoderma.2025.117668

te Pas, E. E. E. M., Hagens, M., and Comans, R. N. J. (2023). Assessment of the enhanced weathering potential of different silicate minerals to improve soil quality and sequester CO_2. *Front. Clim.* 4:954064. doi: 10.3389/fclim.2022.954064

Vicca, S., Goll, D. S., Hagens, M., Hartmann, J., Janssens, I. A., Neubeck, A., et al. (2022). Is the climate change mitigation effect of enhanced silicate weathering governed by biological processes? *Global Change Biol.* 28, 711–726. doi: 10.1111/gcb.15993

Vienne, A., Poblador, S., Portillo-Estrada, M., Hartmann, J., Ijiehon, S., Wade, P., et al. (2022). Enhanced weathering using basalt rock powder: carbon sequestration, co-benefits and risks in a mesocosm study with solanum tuberosum. *Front. Clim.* 4:869456. doi: 10.3389/fclim.2022.869456

Vorrath, M. E., Amann, T., Meyer Zu Drewer, J., Hagemann, N., Aldrich, C., Börker, J., et al. (2025). Pyrogenic carbon and carbonating minerals for carbon capture and storage (PyMiCCS) part II: organic and inorganic carbon dioxide removal in an oxisol. *Front. Clim.* 7:1592454. doi: 10.3389/fclim.2025.1592454

Wei, B., Peng, Y., Lin, L., Zhang, D., Ma, L., Jiang, L., et al. (2023). Drivers of biochar-mediated improvement of soil water retention capacity based on soil texture: a meta-analysis. *Geoderma* 437:116591. doi: 10.1016/j.geoderma.2023.116591

White, A. F., and Brantley, S. L. (1995). Chemical weathering rates of silicate minerals. *Rev. Mineral. Geochem.* 31, 1–581. doi: 10.1515/9781501509650-003

Xiu, L., Gu, W., Sun, Y., Wu, D., Wang, Y., Zhang, H., et al. (2023). The fate and supply capacity of potassium in biochar used in agriculture. *Sci. Total Environ.* 902:165969. doi: 10.1016/j.scitotenv.2023.165969

Xu, Q., Zhang, F., Song, F., Guo, H., Wang, X., Bi, F., et al. (2024). Investigating CO_2 sequestration via enhanced rock weathering: effects of temperature and citric acid on dolomite and basalt. *J. Cleaner Prod.* 485:144414. doi: 10.1016/j.jclepro.2024.144414

Xu, T., Li, H., Vicca, S., Goll, D. S., Beerling, D. J., Chen, Q., et al. (2025). Enhanced rock weathering promotes soil organic carbon accumulation: a global meta-analysis based on experimental evidence. *Global Change Biol.* 31:e70483. doi: 10.1111/gcb.70483

Xu, X., Huang, H., Zhang, Y., Xu, Z., and Cao, X. (2019). Biochar as both electron donor and electron shuttle for the reduction transformation of Cr(VI) during its sorption. *Environ. Pollut.* 244, 423–430. doi: 10.1016/j.envpol.2018.10.068

Yuan, D., Wang, G., Hu, C., Zhou, S., Clough, T. J., Wrage-Mönnig, N., et al. (2022). Electron shuttle potential of biochar promotes dissimilatory nitrate reduction to ammonium in paddy soil. *Soil Biol. Biochem.* 172:108760. doi: 10.1016/j.soilbio.2022.108760